Continental-Scale Landscape Evolution: A History of North American Topography

Victoria M. Fernandes[1], Gareth G. Roberts[1], Nicky White[2] and Alexander C. Whittaker[1]

[1]Department of Earth Science and Engineering, Imperial College London, SW7 2AZ, UK.
[2]Bullard Laboratories, Department of Earth Sciences, University of Cambridge, Madingley Rise, Madingley Road, Cambridge, CB3 0EZ, UK.

Key Points:

- Cenozoic rock uplift history determined from calibrated inverse modeling of 4161 North American river profiles.
- Landscape modeling driven by this uplift history predicts drainage patterns, continental denudation and sedimentary flux histories.
- Incision estimates were tested using continent-wide inventory of thermochronometric measurements.

Corresponding author: Victoria M. Fernandes, v.fernandes17@imperial.ac.uk

Corresponding author: Gareth G. Roberts, gareth.roberts@imperial.ac.uk

This article has been accepted for publication and undergone full peer review but has not been through the copyediting, typesetting, pagination and proofreading process which may lead to differences between this version and the Version of Record. Please cite this article as doi: 10.1029/2018JF004979

©2018 American Geophysical Union. All rights reserved.

Accepted Article

Accepted Article

Abstract

The generation and evolution of continental topography are fundamental geologic and geomorphic concerns. In particular, the history of landscape development might contain useful information about the spatio-temporal evolution of deep Earth processes, such as mantle convection. A significant challenge is to generate observations and theoretical predictions of sufficient fidelity to enable landscape evolution to be constrained at scales of interest. Here, we combine substantial inventories of stratigraphic and geomorphic observations with inverse and forward modeling approaches to determine how the North American landscape evolved. First, stratigraphic markers are used to estimate post-depositional regional uplift. Present-day elevations of these deposits demonstrate that > 2 km of long wavelength surface uplift centered on the Colorado-Rocky-Mountain plateaus occurred in Cenozoic times. Secondly, to bridge the gaps between these measurements, an inverse modeling scheme is used to calculate the smoothest spatio-temporal pattern of rock uplift rate that yields the smallest misfit between 4161 observed and calculated longitudinal river profiles. Our results suggest that Cenozoic regional uplift occurred in a series of stages, in agreement with independent stratigraphic observations. Finally, a landscape evolution model driven by this calculated rock uplift history is used to determine drainage patterns, denudation and sedimentary flux from Late Cretaceous times until the present day. These patterns are broadly consistent with stratigraphic and thermochronologic observations. We conclude that a calibrated inverse modeling strategy can be used to reliably extract the temporal and spatial evolution of the North American landscape at geodynamically useful scales.

1 Introduction

Topography is the result of complex interactions between the solid Earth and surface processes that operate on multiple spatial and temporal scales (e.g. *Anderson and Anderson*, 2010; *Roberts et al.*, 2019). Consequently, surface uplift and subsidence histories have been combined with magmatic and tomographic information to estimate temperatures, wavelengths and timescales of mantle convection (e.g. *Gurnis et al.*, 2000; *van Wijk et al.*, 2010; *Salles et al.*, 2017; *Roberts et al.*, 2018; *Lodhia et al.*, 2018). The results of these studies imply that mantle processes play a significant role in driving the erosional history of a landscape. Unfortunately, existing inventories of uplift or denudation measurements are sparse, which makes it difficult to determine histories of geodynamical processes (e.g. sub-plate support) at appropriate scales. Here, we explore how substantial biostratigraphic and thermochronologic compilations can be combined with stratigraphic information to constrain continental-scale surface uplift histories on time scales of $O(1–100)$ Ma. We match insights from this approach with geomorphic observations to reconstruct a Cretaceous to Recent uplift history of the North American continent where sub-plate processes appear to have played an important role in generating and maintaining long-wavelength topography. Finally, we explore how calibrated rock uplift histories can be used to parameterize three-dimensional forward models of landscape evolution, which make predictions about continental denudation, drainage routing and sedimentary flux that can be assessed using independent geologic observations.

Particular attention is paid to four regions with elevated topography: the Colorado-Columbia-Rocky Mountains plateaus, the Appalachian mountain belt, the Yukon plateau, and the Mexican highlands. Spot measurements of rock and surface uplift (e.g. uplifted marine stratigraphy, stable isotopes, paleoflora, structural geology), denudation (e.g. low temperature thermochronometry, fluvial incision dating) and the geochemistry of basaltic magmatism suggest that a broad region encompassing the Colorado-Rocky Mountain plateaus experienced multi-staged Cenozoic uplift and denudation generated, at least in part, by time-dependent thermal anomalies within the upper mantle (e.g *Sahagian*, 1987; *Flowers et al.*, 2008; *Karlstrom et al.*, 2008; *Huntington et al.*, 2010; *Mix et al.*, 2011; *Chamberlain et al.*, 2012). Punctuated delivery of clastic sediments into the Gulf of Mexico corroborate

©2018 American Geophysical Union. All rights reserved.

Accepted Article

these observations (*Galloway et al.*, 2011). There is also evidence for youthful regional uplift elsewhere. For example, uplifted Pliocene marine sedimentary rocks that crop out along the eastern seaboard and sedimentation rates within the Baltimore Canyon Trough imply that significant topography of the Appalachian mountains may have been generated during the last 20 million years (e.g. *Poag and Sevon*, 1989; *Rowley et al.*, 2013). In the northern cratonic interior, thermochronometric observations and scattered outliers of Cretaceous marine sedimentary rock suggest several hundred meters of post-Cretaceous uplift and denudation occurred (e.g. *Nassichuk and McIntyre*, 1995; *Ault et al.*, 2013). Widespread magmatism, uplifted marine terraces and incised drainage patterns suggest that Mexico also experienced long wavelength Cenozoic uplift (e.g. *Stephenson et al.*, 2014). Nevertheless, the timing and mechanism for generating these patterns of regional uplift remain uncertain.

1.1 A Role for Large-Scale Crustal and Lithospheric Thickening?

Some models explain kilometer-scale changes in continental elevation by invoking crustal thickening by, for example, Early Cenozoic crustal flow (e.g. *McQuarrie and Chase*, 2000). These models have largely fallen out of favor since they are difficult to reconcile with present-day crustal thicknesses estimated from seismic wide-angle surveys, from receiver function analyses and from shear wave dispersion modeling (e.g. *Levander and Miller*, 2012; *Becker et al.*, 2014; *Shen and Ritzwoller*, 2016). Isostatic considerations would require the crust (and by inference the lithosphere) beneath the Colorado Plateau to be 1.7 times thicker than that beneath the Great Plains in order to generate the observed 1.5 km of relief (Figure 1a; *Klöcking et al.*, 2018; Supporting Information). However, empirical parametrization of shear wave tomographic models suggests that the lithospheric thickness beneath the Great Plains is approximately double that of the Colorado Plateau (e.g. *Priestley and McKenzie*, 2006; *Shen and Ritzwoller*, 2016). The striking similarity of crustal thicknesses beneath the Colorado-Columbia-Rocky Mountains plateaus and beneath the Great Plains (35–45 km) is consistent with the view that orogenesis played an insignificant role in generating and maintaining the regional elevation of western North America since Late Cretaceous times [*Spencer*, 1996; *Wilson et al.*, 2005]. The observed velocity structure of the crust indicates that differences in crustal and sedimentary densities alone are insufficient to account for these dramatic changes in topographic relief [*Roberts et al.*, 2012a; *Klöcking et al.*, 2018; *Levandowski et al.*, 2018].

1.2 Epeirogeny and the Role of Dynamic Support

More popular models invoke the development of positive and negative mantle buoyancy anomalies generated by hot upwellings and subducting slabs to generate vertical motions (e.g. *Thompson and Zoback*, 1979; *Humphreys*, 1995; *Spencer*, 1996; *Liu and Gurnis*, 2010; *Karlstrom et al.*, 2012). The admittance, Z, between long-wavelength ($\gtrsim$ 800–2500 km) free-air gravity anomalies and topography for western North America show it has an elastic thickness of 12 ± 3 km, which implies that sub-plate buoyancy anomalies ought to measurably deflect the Earth's surface [*McKenzie*, 2003]. At the longest wavelengths, $Z = 23 \pm 5$ mGal/km, which suggests that the topographies of western North America, the Yukon, Central Mexico and the Appalachian mountains are at least partially supported by sub-plate processes (e.g. *Roberts et al.*, 2012a; *Stephenson et al.*, 2014; Figure 1b). These locations of inferred sub-plate support are corroborated by seismic tomographic imaging, which shows that the upper mantle beneath these parts of North America is anomalously slow and juxtaposed against a central region with thick (> 150 km) lithosphere (e.g. *Priestley and McKenzie*, 2006; *Ritsema et al.*, 2011; *French et al.*, 2013; *Rowley et al.*, 2013; *Molnar et al.*, 2015). Basaltic magmatism coincides with many of these low velocity zones (e.g. Figure 2). Beneath western North America, an overall increase in melt volume at 40 Ma, as well as an abrupt change from lithospheric to asthenospheric signatures at 5 Ma, point towards the emplacement of anomalously hot material during

©2018 American Geophysical Union. All rights reserved.

Accepted Article

the last 70 Ma (e.g. *Fitton et al.*, 1991; *Roy et al.*, 2009; *Klöcking et al.*, 2018; Figure 3). Drainage patterns of the four most prominent topographic swells (e.g. Yukon, western North America, Mexico, Appalachians) are broadly radial, which suggests domal support of the present-day landscape (Figure 1b).

A burgeoning number of geodynamic models have been used to predict mantle flow patterns beneath the continent with a view to constraining the history of dynamic topography (e.g. *Mitrovica et al.*, 1989; *Lithgow-Bertelloni and Gurnis*, 1997; *Liu et al.*, 2008; *Spasojević and Gurnis*, 2012; *Dávila and Lithgow-Bertelloni*, 2015). These models estimate that transient dynamic topography has amplitudes of up to ±2 km and wavelengths of hundreds to thousands of kilometers (see e.g. *Flament et al.*, 2015). They have been used to account for the aerial extent of the Western Interior Seaway as well as for Mesozoic–Cenozoic uplift, subsidence and magmatic patterns (e.g *Rowley et al.*, 2013; *Flament et al.*, 2015; *Liu*, 2015; *Heller and Liu*, 2016). There is considerable debate about how best to parametrize and test these models and it is notable that most of them fail to match the power spectral characteristics of a global database of oceanic residual depth measurements [*Hoggard et al.*, 2016]. Thus, reliable histories of continental-scale vertical motions of the lithosphere are important constraints for this rapidly evolving field.

The purpose of this study is to develop a testable history of uplift and denudation for the North American continent. First, we review published estimates of rock and surface uplift and denudation used to constrain North American topographic growth since Campanian times. We then fill in some of the gaps and omissions by exploiting regional uplift measurements obtained from stratigraphic and biostratigraphic inventories. We generate a continent-wide history of regional rock uplift by inverting an inventory of 4161 river profiles. The calculated rock uplift history is tested using independent stratigraphic data. Finally, we use this uplift rate history to carry out continental-scale landscape simulations whose predictions are tested using a combination of legacy thermochronometric and detrital zircon measurements.

2 General Stratigraphic Constraints

2.1 Birth of the Western Interior Seaway

The chronology of deformed igneous rocks, metamorphic time-temperature paths, low temperature thermochronology and biostratigraphic ages of deformed and overlapping sedimentary rocks testify to the existence of an orogenic belt has spanned the length of the North American continent since Late Jurassic times (see, e.g., *DeCelles*, 2004). Shortening along a $\sim$ 200 km wide and $\sim$ 2000 km long structural belt that is oriented north-south manifests the Sevier orogen [*Gans and Miller*, 1983; *Wernicke*, 1992]. Marine sedimentary rocks deposited within the adjacent Western Interior Seaway provide a useful datum against which Cenozoic uplift can be gauged (e.g. *Ziegler et al.*, 1985; *Sahagian*, 1987). Field mapping, seismic data and borehole penetrations imply that up to 4 km of Late Jurassic to Late Cretaceous marine sedimentary rocks were deposited within the Western Interior basin, indicating that continental flooding was widespread (e.g. Niobrara Formation, Mancos Shale; *Cross*, 1986; *DeCelles*, 1994; *Smith et al.*, 1994; *Setterholm*, 1994; *Nassichuk and McIntyre*, 1995; *Roberts and Kirschbaum*, 1995). These rocks have extensively documented ammonite biozones and known chronostratigraphy (e.g. *Jeletzky*, 1971; *Obradovich and Cobban*, 1975; *Kauffman and Caldwell*, 1993). Sedimentary isopachs and backstripped subsidence curves show that between $\sim$ 92 and 82 Ma the Western Interior basin was narrow and that subsidence patterns are consistent with the growth of foreland basins generated by loading associated with the Sevier orogeny (*Cross and Pilger*, 1978; *Cross*, 1986; *Roberts and Kirschbaum*, 1995; *Pang and Nummedal*, 1995; *Heller and Liu*, 2016). In contrast, subsidence between $\sim$ 80 and 67 Ma occurred over a broader region centered on Colorado and Wyoming. Loading by the Sevier belt or changes in sea level cannot easily account for either the lateral extent or amplitude of observed

©2018 American Geophysical Union. All rights reserved.

Accepted Article

subsidence (*Bond*, 1976; *Pang and Nummedal*, 1995; *Liu and Nummedal*, 2004). A range of geodynamic models have been proposed to explain these subsidence patterns by invoking kilometer-scale Cretaceous dynamic drawdown of large parts of the continent (e.g. *Mitrovica et al.*, 1989; *Gurnis*, 1993; *Liu et al.*, 2008).

2.2 Regression of Western Interior Seaway

By ~ 70 Ma, when peak metamorphism became manifest within the main fold belt, eastward migration of thrust faulting resulted in an increasing partitioning of the Western Interior basin into smaller basins flanked by basement-cored uplifts [*Cross*, 1986; *Dickinson et al.*, 1988; *Stone*, 1993; *DeCelles*, 2004]. This 'Laramide' structural style developed over a wide region east of the Sevier belt (*Dickinson and Snyder*, 1978; *DeCelles*, 2004). Despite the structural relief across these thrusts, intra-basinal deformation is insufficient to denude existing sedimentary deposits or to halt accumulation of Late Cretaceous marine sequences and associated deltaic facies (e.g. *Dickinson et al.*, 1988). At the same time, a Late Cretaceous to Early Paleocene transition from marine deposition (e.g. Pierre shale, Lewis shale) to deltaic (e.g. Fox Hills sandstone) to terrestrial deposition (e.g. Lance formation) facies occurred diachronously across North America (*Dickinson et al.*, 1988; *Lillegraven and Ostresh*, 1988; *Setterholm*, 1994; *Heller and Liu*, 2016). Paleoflow directions of conglomerates from the Laramide intra-montane foreland basins (e.g. Paleocene Ohio Creek Conglomerate, Colorado; Maastrichtian-Paleocene Ojo Alamo Sandstone, New Mexico) indicate that a regional eastward tilt probably existed at ~ 70–60 Ma [*Heller et al.*, 2013]. Late Paleocene to Early Eocene terrestrial, synorogenic conglomerates deposited within the Middle Rocky Mountains record active thrust faulting and erosion (*Fan and Carrapa*, 2014). These combined observations show that during Late Mesozoic to Early Cenozoic times the Western Interior Seaway retreated and substantial parts of western North America were uplifted (*Dickinson et al.*, 1988; *Roberts and Kirschbaum*, 1995). The resultant facies change caused by retreat of this seaway has been linked with variable sedimentary flux, changing styles of subduction, hydration of the lower crust, and dynamic support (e.g. *Kauffman and Caldwell*, 1993; *Humphreys et al.*, 2003; *Dávila and Lithgow-Bertelloni*, 2015; *Levandowski et al.*, 2018). During this period, minor tectonic shortening occurred across the Colorado Plateau (*Spencer*, 1996).

2.3 Post-Cretaceous Events

Thermochronometric and incision rate histories suggest that Cenozoic denudation of the Colorado and Rocky Mountains plateaus occurred in several stages (e.g. *Flowers et al.*, 2008; *Karlstrom et al.*, 2017; *Winn et al.*, 2017). Staged Cenozoic uplift and denudation of North America is consistent with the history of sedimentary deposition observed along the northern and western margin of the Gulf of Mexico [*Galloway et al.*, 2000; *Stephenson et al.*, 2014]. *Feng et al.* [1994], *Peel et al.* [1995] and *Galloway* [2008] showed that that Mesozoic strata in the Gulf of Mexico are relatively uniform in thickness, while Cenozoic sedimentary strata increase in thickness towards the west. The highest rates of sedimentary flux occurred during Paleocene (~ 65 Ma), Oligo-Miocene (~ 40–15 Ma) and Plio-Pleistocene (~ 5–0 Ma Ma) times [*Galloway et al.*, 2011]. Timing of these depositional phases is broadly coeval with the history of uplift estimated from clumped isotopes (Δ_{47}) and with other paleoaltimetric proxies, which imply that the Colorado Plateau had an elevation of 1–2 km between Cretaceous and Oligocene times (e.g. *Gregory and Chase*, 1992; *Wolfe et al.*, 1998; *Huntington et al.*, 2010). *Galloway et al.* [2011], *Blum and Pecha* [2014] and *Blum et al.* [2017] argue that large-scale drainage of the Cordilleran highlands toward the Gulf of Mexico existed by at least Late Paleocene times and that drainage catchments probably extended up to the western flank of the Appalachian mountains. Further west, *Cather et al.* [2008] identified a major denudation event within the Colorado Plateau between the deposition of the Chuska Erg (35–27 Ma) and the Bidahochi Formation (~ 16 Ma).

©2018 American Geophysical Union. All rights reserved.

Accepted Article

Geologic mapping and regional palinspastic reconstructions suggest that the final stages of terrane accretion in Western Canada and Alaska occurred between ~ 50 and 40 Ma and in the Pacific Northwest after ~ 30 Ma, establishing the present-day tectonic configuration of the northwest Cordillera (*Johnston*, 2001; *Dickinson*, 2004). Oxygen isotope paleoaltimetry has been used to suggest that a kilometer-scale 'Nevadaplano' plateau was present in British Columbia by ~ 50 Ma and that it migrated south toward Nevada by ~ 30 Ma (*Chamberlain et al.*, 2012). The presence of an elevated, but low relief, plateau is corroborated by reconstruction of deeply incised, west-flowing paleo-valleys across the present-day crest of the Sierra Nevada [*Best et al.*, 2009; *Cassel et al.*, 2009; *Henry et al.*, 2012]. Cross-cutting relationships of extrusive magmatism and ignimbritic flows, thermochronology together with wide-spread deposition of syn-tectonic basin fill suggest that regional compressive stress gave way to extension stress. The Basin and Range province started to extend at ~ 30 Ma and experienced rapid Miocene (~ 20–15 Ma) stretching and subsidence, coeval with eruption of the Columbia River basalts [*Zoback et al.*, 1981; *Cassel et al.*, 2009; *Colgan and Henry*, 2009; *Chamberlain et al.*, 2012].

The history and chemistry of extrusive western North American magmatism suggest that Cenozoic uplift is related to decompression melting of anomalously warm asthenosphere (Figure 2c; *Snyder et al.*, 1976; *Fitton et al.*, 1991; *Roy et al.*, 2009; *Ferrari et al.*, 2012). The NAVDAT database contains 6713 samples of extrusive magmatism from the Colorado Plateau that suggest a trimodal history with peaks at ~ 70–55 Ma, 40–20 Ma and 6–0 Ma (Figure 3a). Spatio-temporal patterns of magmatism record a westward migration, culminating in a maximum aerial extent during Oligocene times (*Chapin et al.*, 2004). These phases of magmatism are broadly coeval with pulses of sedimentary flux within the Gulf of Mexico between ~ 60–50 Ma, 37–11 Ma and 2–0 Ma (*Galloway et al.*, 2011; Figure 3c). Recent correlation of basalt geochemistry with shear wave velocities suggests that magmatism and uplift of western North America is generated by a thermal anomaly which sits beneath thin lithosphere [*Klöcking et al.*, 2018].

Mexican topography is characterized by an Altiplano-style physiography so that the 1–3 km high Sierra Madre Occidental, the Mexican Altiplano, the Trans-Mexican Volcanic Belt and the Sierra Madre del Sur together form a broad, elevated region (Figure 1a). Reconstruction of an ignimbrite-capped plateau records up to 2 km of incision of the western highlands since 26 Ma [*Montgomery and López-Blanco*, 2003]. The southern portion of this region has peaks that are higher than 5 km. Oligocene ignimbrite flare-ups occurred throughout the Sierra del Sur and migrated southward during Miocene times with a decreasing lithospheric signature (Figure 2a, b; *Márquez et al.*, 1999; *Ferrari et al.*, 1999, 2002; *Ferrari and Bryan*, 2007). Thermal modeling of heatflow measurements suggests that anomalously hot mantle sits beneath the lithospheric plate [*Ferrari et al.*, 2012].

The cratonic interior of North America, including the Canadian Shield, has a modest average elevation ($\lesssim$ 0.5 km; Figure 1a). Backstripping of sedimentary rocks recorded in boreholes shows that it has experienced slow (~ 0.01–0.001 mm a^{-1}) Paleozoic subsidence [*Armitage and Allen*, 2010]. Nonetheless, portions of the Canadian Rockies and of the craton show evidence of youthful uplift. Kimberlites of the Lac de Gras field in central Slave Craton that are ~ 75–45 Ma crop out at 550–600 m elevation. Significantly, these deposits contain xenoliths of marine and terrestrial sedimentary rocks of Albian (~ 113–100 Ma) and Eocene (~ 56–45 Ma) ages, respectively. The present-day absence of cratonic Phanerozoic sedimentary cover suggests that moderate ($\geqslant$ 300 m) uplift and denudation occurred prior to, and after, magmatic emplacement [*Nassichuk and McIntyre*, 1995; *Heaman et al.*, 2004; *Ault et al.*, 2013]. Variations in coal rank from the Upper Cretaceous Plains of Alberta suggest that between 1.1–1.9 km of overburden was removed from the Western Canada basin within the last ~ 60 Ma [*Nurkowski*, 1984; *Bustin*, 1991]. These observations are in agreement with modeling of (U-Th)/He in Apatite (A-He) from the Slave craton, which indicate that regions surrounding the cratonic core of North America

©2018 American Geophysical Union. All rights reserved.

Accepted Article

experienced diachronous post-Cretaceous uplift and exhumation with wavelengths of tens to thousands of kilometers [*Flowers et al.*, 2012; *Ault et al.*, 2013].

The origin of kilometer-scale Appalachian topography remains enigmatic. After the end of rifting at $\sim$ 175 Ma, the eastern seaboard constituted a passive margin (e.g. *Klitgord et al.*, 1988). Long-term slow exhumation rates (20 m Ma^{-1} for $>$ 80 Ma) inferred from AFT measurements are comparable to rates of fluvial erosion estimated using cosmogenic dating. These measurements have been interpreted as evidence for slow and steady decay of an old orogen (cf. *Naeser et al.*, 2004; *Boettcher and Milliken*, 1994; *Pavich et al.*, 1985; *Matmon et al.*, 2003; *Portenga et al.*, 2013). In contrast, A-He thermochronometry suggests that kilometer-scale Late Cretaceous denudation of the southern and northern Appalachians has occurred [*McKeon et al.*, 2014; *Amidon et al.*, 2016]. Topographic relief of the crests of the Appalachian mountains has no obvious relationship to the underlying geologic terranes, which implies that prior tectonic shortening may not be the primary geomorphic control [*McKeon et al.*, 2014].

2.4 Neogene Uplift and Denudation

A range of observations suggest that the Appalachian Mountains experienced Neogene uplift and denudation. Elevation of the warped Orangeburg-Chippenham-Thornburg escarpments and of other reconstructed Cenozoic paleoshorelines record tens of meters of Pliocene to Recent uplift [*Spasojević and Gurnis*, 2012; *Rowley et al.*, 2013]. The shapes of longitudinal river profiles from the southern and central Appalachian Mountains are convex upward, which suggests that this landscape is disequilibrated [*Gallen et al.*, 2013; *Miller et al.*, 2013; *Prince and Spotila*, 2013; *Gallen*, 2018]. Significantly, the Cenozoic stratigraphic record from the adjacent Atlantic shelf shows major pulses of Cretaceous and Miocene sedimentary flux [*Poag and Sevon*, 1989; *Pazzaglia and Brandon*, 1996]. Sedimentary flux estimates are incompatible with slow and steady erosion of the Appalachian Mountains. Thermal modeling of A-He observations show increased Miocene exhumation of this region which correlates with increased sedimentary flux [*McKeon et al.*, 2014]. As *Taylor and Fitzgerald* [2011] and *McKeon et al.* [2014] point out, the lack of post-Cretaceous AFT or A-He ages at other sites does not necessarily preclude Miocene uplift but it does imply that the magnitude of this denudation is small ($\lesssim$ 1 km). In Florida, coarse siliciclastic rocks with a Southern Appalachian provenance overlie Late Miocene carbonate platforms, an observation which is consistent with post-Miocene denudation [*Missimer and Maliva*, 2017]. Detrital zircon analyses from the Atlantic Coastal Plain suggest that the recent erosion in the Appalachian Mountains is related to westward migration of eastern drainage divides [*Naeser et al.*, 2016]. These combined observations indicate that Appalachian physiography is not solely a result of erosional decay of a Paleozoic mountain chain (cf. *Baldwin et al.*, 2003).

Youthful uplift of the northern Appalachian Mountains and of Newfoundland has also occurred. A combination of AFT modeling and $^{40}Ar/^{39}Ar$ ages from Mount Washington in New Hampshire indicates an increased exhumation rate after 60 Ma (*Roden-Tice et al.*, 2012; *Amidon et al.*, 2016). Along the continental margin of Labrador, calibrated seismic profiles show that Mesozoic strata dip seaward and are truncated by Late Oligocene and younger strata, which are consistent with phases of regional uplift (*Dickie et al.*, 2011). A regional Miocene unconformity has also been documented in offshore seismic data (*Ainsworth et al.*, 2014). Subsidence curves and vitrinite reflectance measurements from the Hopedate E-33 well offshore Labrador show that pre-Pliocene strata have been more deeply buried by as much as 750 m prior to removal of Miocene strata (*Japsen et al.*, 2016). Earthquake tomographic modeling has identified a region of slow velocity, which has a diameter of $\sim$ 400 km and is known as the Northern Appalachian Anomaly [*Menke et al.*, 2016]. This anomaly occurs within the asthenosphere beneath southern New England and, if it is of thermal origin, it may play a role in generating youthful uplift.

©2018 American Geophysical Union. All rights reserved.

Accepted Article

In western North America, sedimentary deposits of the Ogallala Group are exposed in the Great Plains and suggest that the eastern margin of the Colorado Plateau was regionally tilted during Miocene times (*McMillan et al.*, 2002). Stratigraphic constraints on the timing of regional tilting places this differential uplift between ~ 6 and 3.7 Ma (*Duller et al.*, 2012). Evidence for younger (i.e. post-8 Ma) regional uplift and surface tilting is corroborated by differential incision of the Rocky Mountains and by a reconstructed low relief surface generated by post-Laramide basin fill, which reached as far east as the Great Plains (*McKenna and Love*, 1972; *McMillan et al.*, 2002). Incision histories of ^{40}Ar/^{39}Ar-dated basaltic flows within the Colorado, Columbia and Rio Grande catchments help to constrain long-term landscape development (e.g. *Wakabayashi and Sawyer*, 2001; *Karlstrom et al.*, 2008, 2017). These catchments have been incised by tens to hundreds of meters during Neogene times (e.g. *Karlstrom et al.*, 2012; *Nereson et al.*, 2013; *Channer et al.*, 2015; *Repasch et al.*, 2017). ^{40}Ar/^{39}Ar dating and magnetostratigraphy of tephra deposits within the oldest marine deposits of the Gulf of California suggests that rifting of the Gulf of California initiated by ~ 7 Ma. Present-day elevations (> 300 m) of the shallow marine Upper Bouse formation implies that uplift of the lower reaches of the Colorado river occurred after ~ 4.8 Ma (*Dorsey et al.*, 2018). Quaternary marine terraces along south-western and eastern coast of Mexico are elevated by several tens of meters above sea level, an observation that is interpreted as a consequence of uplift at rates of up to 3 m ka^{-1} [*Self*, 1977; *Ramirez-Herrera et al.*, 2011].

3 Uplift Histories Inferred from Sedimentary Strata

Elevation of dated marine sedimentary strata is probably the least contentious and most robust constraint on the history of continental uplift. In North America, the distribution of Cretaceous marine rocks, notably the Mancos Shale, provides excellent evidence for kilometer-scale uplift of the Colorado-Columbia-Rocky Mountains plateaus since ~ 80 Ma (e.g. *Ziegler et al.*, 1985; *Sahagian*, 1987; *Roberts and Kirschbaum*, 1995). Specifically, the youngest outcropping marine to terrestrial sedimentary sequences, which mark the latest regressive transitions, provide the key datum against which uplift can be measured.

To determine cumulative uplift histories at spot locations across North America, we exploit an inventory of 4633 unique marine fossil assemblages that have been extracted from the Paleobiology Database (PBDB, `https://paleobiodb.org`). This inventory is focused upon Late Cretaceous and Cenozoic samples which span the last 82 Ma. The PBDB is a substantial, collection-based, occurrence and taxonomic dataset of biota that also contains information about host rock lithology, stratigraphy, age and paleoenvironmental setting. Figure 4a shows the locations of samples exploited in this study. Additional stratigraphic constraints for the timing of uplift initiation were compiled using the methodology of *Dickinson et al.* [1988], which identifies the last marine to non-marine transitions in the sedimentary record. Each regressive sequence is identified from published facies interpretations (e.g. *Roberts and Kirschbaum*, 1995; *Johnson et al.*, 2002; *Gani et al.*, 2015). Locations were determined from state geologic maps (`https://ngmdb.usgs.gov`; Figure 4a). Particular care was taken to identify the lateral and temporal variability of marine to terrestrial transitions, such as those observed for depositional sequences within the Star Point Sandstone, Blackhawk, Castlegate, and Sego Sandstone Formations (e.g. *Gani et al.*, 2015). Stratigraphic ages were assigned using published biostratigraphic and chronostratigraphic sections for the Western Interior Seaway (*Obradovich and Cobban*, 1975; *Merewether and McKinney*, 2015; Figure 4b). The PBDB provides additional constraints for loci of Late Cretaceous paleo-coastlines, which themselves provide a reference paleogeography against which regional uplift can be gauged (*Sahagian*, 1987; *Kauffman and Caldwell*, 1993; *Smith et al.*, 1994; *Roberts and Kirschbaum*, 1995; *Cao et al.*, 2017; Figure 4b).

©2018 American Geophysical Union. All rights reserved.

Accepted Article

At any given location, cumulative uplift, $\int U\mathrm{d}t$, is equal to $z + P \pm S$, where U is uplift rate, t is age, z is present-day elevation, P is paleo-water depth and S is paleo-sea level with respect to present-day mean sea level. Calculated uplift U is both rock and surface uplift and is a minimum value, since any putative subsidence that occurred after deposition cannot easily be determined. Elevation of each sample was extracted from the Advanced Space-borne Thermal Emission and Reflection Radiometer (ASTER) global digital elevation model which has vertical and horizontal resolutions of $\sim$ 20 m and $\sim$ 75 m, respectively (*Tachikawa et al.*, 2011). In each case, elevations are based upon locations reported in the PBDB, which have accuracies of $\pm 0.01^\circ$ which is equivalent to ± 1 km. The greatest source of uncertainty is paleobathymetry. Paleo-water depth ranges were provided for some samples in the database, based on the presence of depth-specific marine fauna (e.g. benthic foraminifera) and indicative sedimentary bedforms. In most cases, paleobathymetry was estimated from the reported environment of deposition and calibrated from marine faunal occurrences (e.g. dinoflagellate cysts, benthic foraminifera), and from geologic descriptions of the formation. The paleobathymetric template described by *Immenhauser* [2009] was assumed (e.g. neritic: 0–150 m; upper bathyal: 150–500 m; middle bathyal: 500–2000 m). Obviously, deltaic and marginal marine deposits have much smaller uncertainties and therefore usually yield better constrained uplift histories. Examples of the biota we used are shown in Table 1 and a comprehensive inventory is provided in the Supporting Information.

Stratigraphic observations of the last marine regression provide the tightest constraints for paleobathymetry since they record the last time the reference surface sat at sea level, for which the paleo-water depth is effectively zero with minimal uncertainty. Many stratigraphic sequences are temporally well defined by ammonite biostratigraphy with uncertainties of ± 0.1 Ma. Figure 4f–n show examples of stratigraphic columns used to estimate regional uplift (Supporting Information). Glacio-eustasy during Late Cretaceous and Paleogene times is not accurately constrained and so we included sea-level change as an additional uncertainty, $\delta S = \pm 50$ m. This uncertainty is probably appropriate for post-Campanian sea-level variations [*Miller*, 2005]. Since all of the stratigraphic and biostratigraphic samples crop out at the Earth's surface, a loading correction for overlying strata is not required (*Sahagian*, 1987). Extremal uncertainties in elevation, paleo-water depth, sea level and sample age were used to estimate uncertainties of average uplift rates, $\overline{U}$, such that

$$\begin{aligned} \overline{U}_{max} &= (P_{max} + Z_{max} + S_{max})/a_{min}, \\ \overline{U}_{min} &= (P_{min} + Z_{min} + S_{min})/a_{max}. \end{aligned} \tag{1}$$

Sample age, a, has a range which primarily depends upon first and last occurrences of the faunal assemblage in question [*Gradstein et al.*, 2012].

Table 1. Biostratigraphic constraints on uplift histories adapted from five samples in the PBDB. CP = Colorado Plateau; RM = Rocky Mountains; GP = Great Plains; AP = Appalachian Mountains; MX = Mexico; Latitude/longitude given in decimal degrees; PWD = paleo-water depth; $\overline{U}$ = average uplift rate (see text). Supporting Information provides detailed fossil occurrences and uplift rate estimates for complete inventory.

Province	Latitude	Longitude	Elevation (m)	Fossil	Age (Ma)	Formation	PWD (m)	$\overline{U}$ (mm /a)
CP	38.9017	-107.9258	1593	*Baculites aquilaensis*	77.05 ± 6.45	Mancos Shale	20 – 200	0.0258 ± 0.00289
RM	40.3166	-107.0333	2310	*Trochocyathus egerius*	69.05 ± 3.05	Lewis Shale	0 – 20	0.0336 ± 0.00179
GP	43.2694	-104.2716	1213	*Baculites baculus*	69.05 ± 3.05	Pierre Shale	15 – 40	0.0179 ± 0.0013
AP	38.8719	-78.5136	283	*Myliobatis dixoni*	61.0 ± 4.0	Nanjemoy	0 – 100	0.00546 ± 0.00184
MX	28.2333	-100.2166	203	*Sphenodiscus aberrans*	68.3 ± 2.3	Escondido	0 – 50	0.00335 ± 0.00123

Compiled uplift constraints are summarized in Figures 4 and 5. Cross sections shown in Figure 4c–e compare present-day elevations of biostratigraphic and stratigraphic constraints with a 100 km wide topographic swath along three key transects. In each case, the

©2018 American Geophysical Union. All rights reserved.

Accepted Article

spatial distribution of samples reveals a broad swell which matches the topography. Figure 5 shows the interpreted paleo-water depth and calculated uplift, which is greater than present-day elevation. Samples used in this study indicate that water depth of the Late Cretaceous Western Interior Seaway was ≤ 300 m (Figure 5a; *Arthur and Sageman*, 2004). These shallow values imply that the present-day elevation of each sample is broadly representative of its cumulative uplift. Our compiled results show that since 80–65 Ma, a region encompassing the Colorado Plateau, Southern Rocky Mountains and swathes of the Great Plains have been uplifted to form a broad swell that has a wavelength of ∼ 1500 km (Figures 4c, 4e and 5b). Calculated uplift reaches a maximum of ∼ 3 km in the Colorado Plateau and Southern Rocky Mountains, decreasing smoothly to ∼ 500 m at the eastern edge of the Great Plains (e.g. Figure 5). The age constraint for initiation of uplift is in general agreement with the proposed start of the Laramide orogeny (*Dickinson et al.*, 1988). Superimposed on this broad swell are shorter wavelength (< 100 km) variations in elevation of up to 1 km, which probably reflect uplift caused by horizontal shortening within the Rocky Mountains (Figure 4c and e; e.g. *Fan and Carrapa*, 2014). In general, however, the correlation between large-scale uplift patterns and individual Laramide structures is tenuous since in many locations there is little difference in cumulative uplift between the Rocky Mountain front and the Great Plains (cf. *DeCelles*, 2004; Figure 5b). A similar pattern is observed for the central and southern portions of the Mexican Highlands where 1.5–2.5 km of post-Cretaceous uplift decreases smoothly toward the Gulf coast and toward the Basin and Range province. Sample density makes it difficult to distinguish smaller scale uplift patterns.

Along the Gulf and Atlantic Coastal Plains, sedimentary successions containing marine fossils were deposited on a shallow marine shelf, at the shoreface, or within a deltaic environment. In general, they record seaward progradation of the continental shelf (Figure 5a; *Olsson et al.*, 1988; *Gohn*, 1988; *Pazzaglia and Gardner*, 1994). Figure 4d shows Late Cretaceous to Eocene age samples from the Gulf Plain region at elevations of ∼ 200 m. Here, calculated uplift smoothly increases westward towards the Mexican Highlands where Cretaceous samples from the Rio Grande Embayment are at an elevation of 500 m. Regional tilt of the eastern Gulf Coast and Atlantic Coastal Plain samples (Figure 4d and e; stratigraphic columns j, k and n) is suggestive of long-wavelength (∼ 1000 km) surface uplift of magnitude ≤ 300 m that has developed since Eocene times. Regional uplift calculated for samples along the Pacific Coastal Ranges reveals no simple large-scale pattern, which probably reflects the complex tectonic history of terrane accretion, lateral displacement, subduction and subsidence (e.g. *Awater*, 1970).

The magnitude of regional uplift across the Colorado Plateau, Mexico and the Appalachian Mountains is obviously too great to be accounted for by glacio-eustasy (cf. *Miller*, 2005). Figure 4c-e shows the pattern of maximum and minimum free-air gravity anomalies, which broadly mimics topographic elevation. Long wavelength (> 1000 km) post-Cretaceous warping of North American topography and the co-location of gravity anomalies, slow shear wave velocity anomalies, and magmatic observations indicate that sub-plate support has played a significant role in generating and maintaining kilometer-scale Cenozoic epeirogeny of large portions of North America (cf. Figures 1 & 2). Despite the spatial and temporal coverage provided by the PBDB, there are extensive tracts where uplift histories are poorly understood since it is difficult to interpolate between spot measurements. A potentially fruitful approach is to exploit drainage patterns, which are ubiquitous throughout the continent.

4 Geomorphic Considerations

In principal, drainage networks should indirectly record uplift histories although this record is obscured by the erosional process (e.g. *Howard*, 1994; *Whipple and Tucker*, 1999; *Snyder et al.*, 2000; *Kirby and Whipple*, 2001; *Wobus et al.*, 2006). Significant effort has been put into developing techniques that can be used to extract information about

©2018 American Geophysical Union. All rights reserved.

Accepted Article

geologic and geomorphological processes from fluvial networks. Many modeling studies have shown that the shape of a river profile is affected by changes in uplift rate, which acts to generate transient knickzones (e.g. *Howard and Kerby*, 1983; *Rosenbloom and Anderson*, 1994; *Crosby and Whipple*, 2006). It is evident that longitudinal rivers profiles from multiple catchments share common knickzones, which suggests that uplift rate can affect whole catchments (e.g. *Roberts et al.*, 2012b; *Roberts et al.*, 2019). In this study, we apply a general inverse approach that enables regional rock uplift rates as a function of time and space to be extracted from large inventories of river profiles [*Rudge et al.*, 2015]. This approach has four important steps. First, continent-wide drainage patterns are extracted from a suitable digital elevation model and their veracity checked using satellite imagery. Secondly, a physically appropriate erosional model is chosen. Thirdly, the erosional constants used in this model are calibrated and the drainage inventory is inverted to determine the smoothest rock uplift rate history that minimizes the misfit between observed and calculated river profiles. It is crucial that the calculated rock uplift history is carefully tested using independent geologic observations. Finally, the calibrated uplift rate history can be used to parameterize landscape evolution models that make testable predictions about regional denudation and sedimentary flux, which allows us to examine sensitivities of drainage planforms to calculated uplift. Each of these steps is tackled in the following way.

4.1 Drainage Inventory

An inventory of 4161 river profiles was extracted from the ASTER GDEM database. Rivers were extracted from cells with calculated upstream drainage areas larger than 4 km^2. Esri flow-routing algorithms were used to calculate overland flow, which in turn enables river profiles to be constructed. The planform drainage network was compared to satellite imagery (e.g. Copernicus, Landsat) and it can be shown that the extracted network has high fidelity in regions away from flat topography and narrow ($<$ 30 m wide) gorges. Figure 1b shows the drainage distribution for North America, which is radially distributed about four major topographic swells: the Yukon plateau (centered on 60° N and 140° W), the Colorado-Columbia-Rocky Mountains plateaus (45° N and −05° W); Mexico (20° N and 100° W); and the Appalachian mountains (35° N and 80° W).

Families of longitudinal river profiles grouped by catchment are shown in Figure 6. Profiles from the Colorado catchment exhibit two substantial convexities at $\sim$ 500–1000 km and at $\sim$ 1500–2500 km (Figure 6). River profiles from the Columbia catchment and from the upper western reaches of the Mississippi catchment also have substantial knickzones (Figure 6). Pronounced convexities are observed on river profiles that drain northern and eastern North America (e.g. at $\sim$ 1500–2000 km along the Nelson river). Many other North American catchments also have large convex-upward knickzones. The locations of these broad knickzones do not generally correlate with lithologic contacts, which suggests that their shapes are not related to substrate (e.g. bedrock) in a simple way [*Roberts et al.*, 2012a]. Instead, the observed commonalities of long wavelength knickzones draining the four topographic swells suggests that they could have been generated by the spatial and temporal pattern of regional uplift.

4.2 Erosional Parametrization

Shapes of longitudinal river profiles, $z(x)$, are controlled by the history of rock uplift rate, U, and by erosion rate, E, both of which can vary as a function of space, x, and time, t (e.g. *Gilbert*, 1877; *Davis*, 1899; *Howard*, 1994; *Whipple and Tucker*, 1999; *Sklar and Dietrich*, 1998; *Loget and Van Den Driessche*, 2009; *Anderson and Anderson*, 2010). A range of laboratory experiments and field measurements suggest that erosion rate depends upon a suite of complex processes that include the dynamics of water flow (e.g. discharge, turbulence, vorticity), strength of the substrate (e.g. bedrock), orientation of jointing and fracturing, local erosional mechanisms, sediment supply and biota (e.g. *Sklar*

©2018 American Geophysical Union. All rights reserved.

Accepted Article

and Dietrich, 1998, 2001; *Brocard and Van Der Beek*, 2006; *Allen et al.*, 2013; *DiBiase et al.*, 2014; *Mackey et al.*, 2014; *Rengers and Tucker*, 2014; *Castelltort et al.*, 2015; *Brocard et al.*, 2016; *Baynes et al.*, 2018).

At continental scales, it appears that large, coherent signals become emergent and that the stream power equation provides a practicable way to model drainage evolution through time and space (e.g. *Roberts et al.*, 2019). For example, at wavelengths > 10 km, lithology does not appear to correlate with changes in slope, with curvature or with stream power [*Roberts et al.*, 2012a; *Czarnota et al.*, 2014]. These inferences are consistent with spectral analyses of river profiles, which suggest that processes operating at long wavelengths (> 100 km) dominate the shapes of river profiles [*Roberts et al.*, 2019; *Roberts*, 2019]. Assumptions of erosional thresholds do not seem to be required in order to achieve a good match between observed and calculated river profiles at these long wavelengths [*Roberts et al.*, 2012a]. Furthermore, changes in precipitation rate where the period is less than about 1 Ma do not significantly affect calculated river profile shapes (e.g. *Paul et al.*, 2014). Fluvial erosion appears to be a highly integrative process such that regional uplift primarily determines profile shape. The empirical stream power equation is given by

$$\frac{\partial z(x,t)}{\partial t} = -vA(x)^m \left(\frac{\partial z(x,t)}{\partial x} \right)^n + U(x,t), \tag{2}$$

where upstream drainage area A varies as a function of distance, x. z is elevation above sea level, t is time and U is rock uplift rate. Values of the erosional constants v, m and n can be determined by independent calibration. Equation (2) can be solved in order to calculate U. For example, *Pritchard et al.* [2009] demonstrated that U can be extracted from river profiles by exploiting the method of characteristics. Later, *Royden and Perron* [2013] employed the same integrative approach to calculate metrics that may relate to landscape evolution. These metrics, notably τ_G and χ, are often used to gauge the time taken for erosional signals to propagate through a given landscape and to infer drainage divide migration. A challenging problem is that regional uplift signals are generally inserted into the upstream reaches of individual rivers and catchments. An obvious solution is to pose the inverse problem whereby a smoothly varying rock uplift rate history, $U(x, y, t)$, is sought. The problem can be solved by either linear or non-linear optimization. We assume that drainage area is temporally invariant, which implicitly assumes that reorganization of planform does not significantly affect shapes of rivers at the scales of interest [*Paul et al.*, 2014; *Rudge et al.*, 2015]. Significantly, no *a priori* assumptions about the spatial and temporal distribution of uplift signals are made. An inverse approach provides a pragmatic and testable way to calculate rock uplift rate histories at scales appropriate for investigating histories of sub-plate support.

4.3 Inverse Modeling

The inverse scheme proposed by *Pritchard et al.* [2009] was generalized to incorporate 'erosional diffusivity' and spatio-temporal changes in uplift rate histories by exploiting quasi-linear optimization methodologies [*Roberts and White*, 2010; *Roberts et al.*, 2012b]. A significant benefit of non-linear inverse modeling is that it is possible to investigate the importance of erosional parameters whose values are much debated [*Lague*, 2014]. For example, a suite of inverse models shows that residual misfit is minimized when the slope exponent, n, equals 1 [*Paul et al.*, 2014]. This result means that a simplified erosional model can be used to develop a linearized inverse model using a Bayesian approach in which *a posteriori* probability distributions (e.g. prior guesses at approximate rock uplift histories) are defined and, alternatively, a damped linear least squares approach that has a null starting set [*Fox et al.*, 2014; *Goren et al.*, 2014; *Rudge et al.*, 2015]. Other schemes have also been proposed (e.g. *Campforts and Grovers*, 2015; *Glotzbach*, 2015).

©2018 American Geophysical Union. All rights reserved.

Accepted Article

Rudge et al. [2015] show that smooth spatio-temporal rock uplift histories can be obtained by linear inverse modeling without recourse to prior information. By solving the simplified stream power equation using the method of characteristics, the landscape response time, τ_G, can be expressed as

$$\tau_G - t = \int_0^{x(t)} \frac{\mathrm{d}x}{vA^m}. \tag{3}$$

Elevation is given by

$$z^* = \int_0^{\tau_G} U(x(t), t)\mathrm{d}t, \tag{4}$$

[*Luke*, 1972; *Weissel and Seidl*, 1998]. The resultant set of linear equations that relate elevation to rock uplift and erosion is rewritten in matrix form as

$$\mathbf{z} = \mathrm{M}\mathbf{U}. \tag{5}$$

Families of river profiles are inverted by minimizing

$$|\mathrm{M}\mathbf{U} - \mathbf{z}|^2 + \lambda_S^2|\mathrm{S}\mathbf{U}|^2 + \lambda_T^2|\mathrm{T}\mathbf{U}|^2. \tag{6}$$

where S and T are the spatial and temporal smoothing matrices, respectively [*Rudge et al.*, 2015]. U is permitted to vary subject to a non-negativity constraint, $\mathbf{U} \geq 0$, since river profile elevations constitute positive measurements. Uplift rate is allowed to vary as a function of time at vertices arranged in a triangular grid with a spacing of 125 km. The starting set is the null set and and we make no assumption about pre-existing North American paleotopography. Uplift along river profiles is linearly interpolated from this spatio-temporal grid. It is important to note that the model cannot resolve uplift rate at times that are greater than the largest value of τ_G. Following *Parker* [1994]'s protocol, the spatial and temporal smoothing coefficients, λ_S and λ_T, are systematically varied to identify the smoothest model that yields the best fit between observed and calculated river profiles (Figure 8). Here, we used $\lambda_S = 0.5$ and $\lambda_T = 0$ and the effective temporal resolution is just under 6 Ma. Different values of λ_S and λ_T have also been tested.

One way to constrain the value of m is to calculate residual misfit from a suite of inverse models for which m is systematically varied. In each case, it is important to ensure that the same number of free parameters is used. In essence, this approach exploits the spatial geometry of drainage networks (i.e. $A(x)$) to constrain m. Crucially, we allow rock uplift to vary spatially and temporally, which means signals can be inserted at any position along different river profiles and we do not assume river profiles are in steady state (i.e. $\partial z/\partial t = 0$). Indeed, we caution against the use of methodologies which assume steady state, which exploit the derivative of river profiles, or which prescribe an *a priori* uplift history. In general, all three of these assumptions yield unstable and misleading results. Figure 8 shows that North American river profiles are consistent with an optimal value of $m = 0.4$, although the range $0.2 \leq m \leq 0.5$ has sufficiently small residual misfits to be deemed acceptable. The value of v, which trades off against m, was calibrated using the history of incision recorded by eroded lava dams within the Grand Canyon [*Karlstrom et al.*, 2008]. The mean incision rate is 111 ± 7 m Myr^{-1}. By combining this rate with local slope and area measurements *Roberts et al.* [2012a] showed the relationship between erosional parameters v and m is $v = 4.16 \times 10^4 \times (2.78 \times 10^{-12})^m$. For $m = 0.4$, v has a value of 0.99 ± 0.062 m$^{0.2}$ Myr^{-1}. We explore the impact of changing v by plus or minus one order of magnitude (Supporting Information).

The optimal fit between observed and calculated river profiles shown in Figure 6 is obtained for the cumulative rock uplift history shown in Figure 7. The root-mean-squared (rms) misfit is given by

©2018 American Geophysical Union. All rights reserved.

Accepted Article

$$\left[\frac{1}{N}\sum_{i=1}^{N}\left(\frac{z_i^o - z_i^c}{\sigma}\right)^2\right]^{1/2}, \tag{7}$$

where N = number of data values, z^o and z^c are observed and calculated river elevations, respectively. Elevation variance was set as a constant value of $\sigma = 20$ m, based upon the reported resolution of the ASTER database (*Tachikawa et al.*, 2011). We emphasize that alternative objective functions can be used to measure the goodness of fit between observed and calculated river profiles without significantly affecting our principal results. Finally, we note that our approach does not explicitly address the difficult problems of internal drainage or of strike-slip tectonics, which means that calculated uplift histories along the Pacific seaboard and Great Basin should be treated with caution.

4.4 Calculated Rock Uplift History

The calculated uplift history is shown in Figure 7. This history yields a residual rms misfit of 1.25 between observed and calculated river profiles. The most striking feature of this history is the Cenozoic growth of topography in western North America which can be divided into two principal uplift events. Between ~ 80 and 40 Ma, regional uplift rate is modest, rarely exceeding ~ 0.02 mm/a. Between 30–20 Ma and the present day, uplift rate dramatically increases and reaches values as high as 0.1 mm/a. This calculated history predicts that the Colorado-Columbia-Rocky Mountains plateaus was uplifted from approximately sea level (i.e. < 250 m) at ~ 80 Ma to an average elevation of 1.5–2.5 km at the present day. Note that the Rocky Mountains front and the Great Plains are uplifted at approximately the same time. Late Cretaceous to Recent cumulative uplift reaches 2.5–3.0 km within the southern Rocky Mountains, decreasing northward to ~ 1.5 km toward the Canadian Rockies and eastward to 0.5–1.0 km toward the Great Plains. Along the southern slopes between the Rocky Mountains and the Great Plains, cumulative uplift appears to have occurred in two broadly synchronous pulses between 60–40 Ma and 20–0 Ma. Regional uplift is progressively younger and of shorter duration toward the north. The southern portion of the Great Plains becomes emergent after 20 Ma.

With the exception of the Rio Grande Embayment, calculated cumulative uplift along the Gulf Coastal Plain is < 250 m. Between Georgia and the Mississippi Embayment, a rapid episode of regional uplift occurs at ~ 35 Ma. A cumulative uplift of 400 m is predicted to have occurred within the last 20 Ma for the Rio Grande Embayment with fastest uplift rates between 20 and 10 Ma. Post-Cretaceous uplift of the Mexican Highlands generally exceeds 1 km. The southern and northernmost portions of these highlands were uplifted by almost 3 km and ~ 2 km, respectively. Along the eastern seaboard, our results suggest that the central Appalachian mountains were uplifted by ~ 1 km. The adjacent coastal plain underwent a maximum uplift of 300 m. Within cratonic North America, cumulative uplift is modest which suggests that the Canadian Shield and Interior lowlands have sat at relatively low elevation since Late Cretaceous times.

4.5 Independent Tests

A significant advantage of an inverse modeling approach is that the predicted regional rock uplift as a function of space and time can be tested against independent observations. Here, we have carried out this testing by comparing predicted uplift histories with those determined from the biostratigraphic and stratigraphic inventory (Figure 4). The average uplift rate at each location was estimated from the age and elevation of the biostratigraphic sample. This value can be directly compared with the average predicted uplift rate, which is determined from the amount of cumulative uplift that has occurred since the time of deposition. We did not use samples that are younger than 5 Ma since the temporal resolution of the calculated uplift history is of O(5–10) Ma (Figure 7).

©2018 American Geophysical Union. All rights reserved.

Accepted Article

Comparison between observed stratigraphic and biostratigraphic constraints, and predicted average uplift rate measurements are presented in Figure 9. Analysis of the smaller stratigraphic database shows that the inverse model yields a good agreement between observed and predicted uplift rates. Figure 9b presents a similar set of results for the much larger PBDB inventory. Open white circles comprise observations with relatively small uncertainties that are within an order of magnitude of the central value. In these cases, observed and predicted values agree to within a factor of two. Gray circles also agree but have large observed uncertainties, principally because of relatively poorly constrained paleobathymetry. We conclude that calculated average uplift rates for most of the Colorado-Columbia-Rocky Mountains plateaus, the Appalachians, Texas, Mexican Highlands, Yukon and the Great Plains are consistent with a combination of biostratigraphic and stratigraphic uplift measurements (Figure 9c,d).

There are two regions where the inverse model significantly over- or under-predicts observed uplift rates: the Pacific Coastal Ranges and the Rio Grande Embayment. It is unsurprising that a damped inverse model yields a poorer fit along the Pacific Coast, which has experienced a complex tectonic history dominated by transcurrent plate motions and regional subsidence (e.g. *Awater*, 1970; *Bartow*, 1991). Over-predicted uplift rates within the Rio Grande Embayment are more problematic. The biostratigraphic compilation indicates that this embayment progressively shallowed from a deep marine Upper Cretaceous environment until Late Eocene times when deposits were predominantly deltaic or estuarine (e.g. Wilcox Formation; *Galloway*, 2001; *Milliken et al.*, 2018). Since then, this region probably remained close to sea level, manifest by a record of Cenozoic shoreline progradation along the Coastal Plain (*Hosman*, 1996; *Galloway*, 2001). At present, the embayment is adjacent to the uplifted Sierra Madre province. Since relatively few rivers drain this region, there is lower model coverage, which is a possible reason why regional uplift has been over-predicted (Figures 1b, 7). We note that if the prefactor of the stream power relationship, v, is either decreased or increased by one order of magnitude, the resultant uplift history yields calculated rates that significantly mismatch stratigraphic and biostratigraphic constraints. These tests suggest that our calibrated value of v is a reasonable one (Supporting Information).

An assessment of model fidelity can also be made using additional independent uplift constraints (e.g. number of recorded extrusive events, clumped-isotope constraints). A two stage Cenozoic uplift history of the Colorado Plateau is consistent with paleoaltimetric observations calculated from clumped isotopic analysis [*Huntington et al.*, 2010]. The distribution of extrusive magmatic events summarized in the NAVDAT database displays two broad peaks at $\sim$ 80–55 Ma and at $\sim$ 40–0 Ma (see e.g. *Chapin et al.*, 2004). In Alaska, three phases of magmatism centered at 33, 15 and 2 Ma have been recorded (Figure 2). Timing of peak magmatism is consistent with changes of predicted uplift rates (Figure 7b). In southern North America and Mexico, predicted regional uplift is consistent with the distribution of Cretaceous marine sedimentary rocks (Figure 4a; *Bond*, 1976; *Sahagian*, 1987). Along the Atlantic margin, Cretaceous marine sedimentary rocks also crop out which is consistent with calculated regional uplift since the age of deposition. Between 30°N and 35°N, the elevation of an emergent Pliocene marine terrace increases from 20–30 m to 60–80 m (*Rowley et al.*, 2013). Calculated cumulative uplift in this region increases from $\sim$ 40 Ma with higher rates between 30 Ma and the present day (Figure 7b).

The inverse model yields a good match to 100% and 86% of the stratigraphic and biostratigraphic inventories, respectively. We conclude that a continent-wide spatial and temporal uplift history calculated by inverting an inventory of 4161 river profiles generally agrees with a suite of independent constraints. Our results build upon, and are consistent with, non-linear inverse modeling of a much smaller inventory of 93 river profiles [*Roberts et al.*, 2012a].

©2018 American Geophysical Union. All rights reserved.

Accepted Article

5 Landscape Modeling

The inverse modeling procedure that we have described and applied can be further tested by landscape modeling. By forcing a landscape evolution model with the rock uplift rate history calculated by inverse modeling, testable predictions about elevation, drainage patterns, denudation and sedimentary flux are made. In particular, the way in which the planform of drainage patterns evolves as it responds to regional uplift can be examined. In future, it may prove possible to directly invert continental-scale topography for uplift and denudation using a landscape evolution model (e.g. *Croissant and Braun*, 2014). At present, guided forward modeling is a pragmatic and computationally efficient approach for calculating continental-scale landscape evolution.

5.1 Badlands Algorithm

A modified version of the Basin and Landscape Dynamics (Badlands) model is used to calculate the spatial and temporal evolution of North American topography during the last 82 Ma together with discharge, denudation and sedimentary flux [*Salles*, 2015]. This landscape evolution model exploits a triangular mesh to solve the relevant geomorphic equations. Here, this mesh is generated from vertices with a regular spacing of 10×10 km. Drainage flow paths were determined using a single flow direction, steepest descent algorithm. Volumetric sedimentary flux was calculated across cell edges. The time steps are determined in accordance with a Courant-Friedrichs-Lewy condition to ensure numerical stability. As proposed by *Salles* [2015] a diffusion coefficient, $\kappa = 10^{-20}$ m^2 Ma^{-1}, is included to ensure model stability. We purposefully ensured that the forward model is kept as simple as possible and that the three erosional parameters, v, m and n, have identical values to those used for inverse modeling. Fixed Dirchlet boundary conditions were employed along the edges of the box to ensure that no interference with drainage development of the continental domain occurred. The model was not permitted to deposit sediment on the continent or along its margins, sea level was assumed to be constant and precipitation rate, P, was set at unity. Finally, flexural responses to repartitioning of surface loads, glacial erosion and ice cover were not included and we made no corrections to the loci of paleo-shorelines (cf. *Wickert*, 2016; *Salles et al.*, 2017). The governing empirical equation takes the form

$$\frac{\partial z}{\partial t} = -v(AP)^m \nabla z - \kappa \nabla^2 z + U(x, y, t), \tag{8}$$

where U is the rock uplift rate history that was previously obtained by inverse modeling of the drainage inventory (Figure 7a). Incision rates (i.e. $\partial z/\partial t - U$) are easily extracted from numerical solutions of Equation 8. In turn, these rates can be used to calculate cumulative denudation at spot locations by integrating incision rate with respect to time or to calculate sedimentary flux by integrating with respect to flow length in a downstream direction. We investigated the impact of four initial conditions on channelization and subsequent drainage planforms: a random distribution of slopes with small (i.e. meter-scale) relief, and 1%, 5% and 10% of present-day topography (Supporting Information). These percentage fractions of present-day topography were calculated by multiplying the ASTER GDEM grid by 0.01, 0.05 and 0.1, respectively. By etching the initial condition (i.e. starting topography), the initial drainage pattern is set which subsequently evolves as the landscape develops. The impact of alternative uplift histories on calculated landscape evolution was investigated by rotating inserted rock uplift patterns by 90°. This test broadly preserves the amplitude-frequency content of inserted uplift (Supporting Information).

5.2 Calculated Landscape

Figure 10 presents elevation, discharge (i.e. drainage networks), cumulative denudation and sediment load as a function of geologic time for the last 70 Ma for a Badlands

©2018 American Geophysical Union. All rights reserved.

Accepted Article

model that has a 5% initial condition. Unsurprisingly, this model predicts elevations at the present day that are similar to the ASTER GDEM topography (Figure 10a). In some locations, calculated elevations are lower than observed, especially within the Appalachian Highlands and Canadian Rockies, which we attribute to model smoothing. Calculated Cenozoic discharge suggests that the major continental-scale catchments (e.g. Mississippi, Colorado, Columbia, Yukon, Mackenzie) are broadly stable. For example, most of the large rivers that drain western North America into the Gulf of Mexico have similar flow patterns over the last ~ 65 Ma, which is consistent with zircon provenance measurements from Cretaceous and Paleocene fluvial sandstones along the northern margin of the Gulf of Mexico (Figure 2; *Blum and Pecha*, 2014; *Blum et al.*, 2017). Similar results have been obtained for the random slope condition and for the 1% initial condition. Drainage planforms are more entrenched for the 10% initial condition (Supporting Information). One concern is that the cell size used to parameterize the landscape evolution model can potentially force the drainage planform to remain fixed [*Goren et al.*, 2014]. This concern was examined by changing the inserted rock uplift history. In these tests, the initial condition (5% of present-day topography) was kept the same as for the earlier test. Results show that calculated planforms (e.g. rivers and drainage divides) do indeed adjust and change as the landscape develops, in accordance with the pattern of forcing uplift.

5.3 Denudational History

Thermochronometric measurements provide an additional means of estimating denudation over long time scales. In essence, these techniques record the temperature of rocks as a function of time. By relating these histories to estimates of crustal temperatures, it is possible to extract denudational histories (see e.g. *Green et al.*, 1989; *Gleadow and Brown*, 1999; *Gallagher*, 1995; *Farley*, 2002). A key result from thermochronometers is the age at which rock has cooled below the closure temperature of the individual system. The presence of cooled rock at Earth's surface today is usually interpreted as removal of overburden by denudation. We have tested our predicted denudation history by exploiting the results from two well-known low-temperature thermochronometers: apatite fission track (AFT) and apatite (U-Th)/He (A-He). Our principal aim is to investigate how well the landscape evolution model, which was parameterized using a smoothly varying rock uplift history, can reproduce independent estimates of exhumation. Our compilation of thermochronometric results builds on previous inventories and includes 1642 AFT and 789 A-He closure ages from North America (e.g. *Sloan et al.*, 2003; *Herman et al.*, 2013; USGS National Geochronology Database; Supporting Information). The spatial and temporal distribution of this compilation is presented in Figure 11a–d. We have attempted to identify samples with cooling histories that have been overprinted by tectonic and/or magmatic events and manually excised them from the compilation.

Figure 11d shows there are three broad peaks evident within AFT closure age measurements: 80–60 Ma, 50–30 Ma and 30–10 Ma. The number of measurements of A-He closure ages is greatest between ~ 20 Ma and the present day. Thermobarometric modeling and rock cooling histories suggest that Cenozoic denudation rates across southern North America and Mexico were highest during the last 40 Ma [*Gray et al.*, 2001; *Montgomery and López-Blanco*, 2003; *Ferrari et al.*, 2012]. One interpretation of this trimodal distribution is that North America has experienced at least three discrete kilometer-scale phases of Late Mesozoic to Recent denudation. However, we acknowledge that this database has significant spatial bias; coverage is greatest on the Colorado-Columbia-Rocky Mountains plateaus, along parts of the Appalachian mountains, Mexican highlands, and within the Yukon region (Figure 11a and b). Portions of the Colorado Plateau that have a two-stage Cenozoic cooling history have been interpreted as evidence for an ancestral Colorado river. We note that alternative explanations exist (see, e.g., *Flowers and Farley*, 2012; *Karlstrom et al.*, 2014). Late Cretaceous to Early Paleocene A-He and AFT ages along the Appalachian mountains suggest that ~ 2 km of overburden has been removed during the last ~ 60 Ma. Closure ages along the northern Pacific Coastal Ranges are

©2018 American Geophysical Union. All rights reserved.

Accepted Article

mostly younger than 50 Ma. In the north and central Rocky Mountains, closure ages are between 70 and 40 Ma, which is broadly coeval with the timing of Laramide tectonism (e.g. *Dickinson et al.*, 1988; *Peyton and Carrapa*, 2013). In the Southern Rockies and Rio Grande Rift, there are a suite of A-He and AFT closure ages < 40 Ma. *Kelley and Chapin* [1995] and *Peyton and Carrapa* [2013] related this post-Laramide cooling to burial, subsequent epeirogenic uplift and removal of sedimentary rocks while the Rio Grande Rift developed. *O'Sullivan and Currie* [1996] and *O'Sullivan and Lane* [1997] propose that the Yukon plateau has had a staged denudation history, with cooling phases between 60 and 40 Ma, and at ~ 15 Ma.

In order to compare this compilation with our predictions, we first convert reported closure ages into average denudation rates. Temperature histories of rocks can be extracted by inverting apparent ages and fission track length distributions [*Ketcham*, 2005; *Gallagher*, 2012]. However, it is still unclear how spatial averaging of cooling histories, rates of exhumation at the time of closure and time-dependent geothermal gradients affect these results [*Schildgen et al.*, 2018]. Here, we use a simple expression that relates surface and closure temperatures, T_s and T_c, geothermal gradient, $\mathrm{d}T/\mathrm{d}z$, and closure age, a_c, in order to calculate the time-averaged denudation rate which is given by

$$\frac{\mathrm{d}z}{\mathrm{d}t} = \frac{T}{a_c(\mathrm{d}T/\mathrm{d}z)}, \tag{9}$$

where $T = T_c - T_s$. Measurement errors and uncertainties in the thermal properties of the crust were propagated to obtain

$$\delta_{\mathrm{d}z/\mathrm{d}t} = \left|\frac{\mathrm{d}z}{\mathrm{d}t}\right| \sqrt{\left(\frac{\delta_T}{|T|}\right)^2 + \left(\frac{\delta_{\mathrm{d}T/\mathrm{d}z}}{|\mathrm{d}T/\mathrm{d}z|}\right)^2 + \left(\frac{\delta_{a_c}}{|a_c|}\right)^2}, \qquad \delta_T = \sqrt{(\delta_{T_c})^2 + (\delta_{T_s})^2}. \tag{10}$$

These errors can also be gauged by using extremal values of the variables. Significant uncertainties include closure temperatures, which vary between 110 ± 10°C for AFT and ~ 60 ± 30°C for A-He, although a larger range for AFT is sometimes reported [*Dodson*, 1973; *Green et al.*, 1989; *Reiners and Brandon*, 2006]. Geothermal gradients can be affected by changes in basal heat flow, by the distribution of radiogenic elements, and by thermal advection. We tested a suitable range of geothermal gradients (25 ± 15°C km^{-1}), which broadly encompasses those values reported for radiogenic to weakly radiogenic crust. These values are the most significant control for crustal temperatures of unstretched lithosphere (e.g. *McKenzie et al.*, 2005). Surface temperatures are often poorly constrained and we assumed that T_s = 15 ± 10°C (see e.g. *Greenwood and Wing*, 1995). We acknowledge that more complex thermo-kinetic models exist which incorporate, for example, the effects of two- and three-dimensional conductive cooling and advection of heat (e.g. *Braun*, 2002). In our view, the uncertainties in thermal structure of the crust and its time-dependent behavior mean that simple models are justifiable in this instance. For each sample, denudation rate and associated error were calculated using Equations 9 and 10 (Supporting Information).

It is important to emphasize that rock uplift without concomitant denudation is difficult to detect using thermochronometric techniques. Conversely, rapid erosion can in principal produce significant denudation in the absence of surface uplift. One way to examine the cause of rock cooling and its relationship with uplift is to extract denudational estimates from parametrized landscape evolution models. Here, we use the compilation of rock cooling rates to test predicted values (Figure 10). It is important that these rates are compared at the same location and for the timescale determined by the closure age of the thermochronometric measurement. We avoided comparing samples with closure ages younger than 6 Ma which is the limit of resolution for our landscape model. Furthermore, young AFT (or AHe) ages that are <5 Ma can be affected by thermal advection which we have ignored for simplicity [*Lisker et al.*, 2018]. A comparison between observed and

©2018 American Geophysical Union. All rights reserved.

Accepted Article

predicted denudation rates is presented in Figure 11e and f. For clarity, uncertainties are shown for samples where our model matches thermochronometric measurements within error (plus or minus a factor of two), representing 90% of the A-He and 36% AFT samples in our inventory. Samples where denudation cannot be predicted within error are shown as blue circles. The landscape evolution model under-predicts 10% and 64% of the A-He and AFT measurements, respectively. One way to interpret these results is that A-He closure ages are more closely related to the formation of the modern landscape than AFT measurements. Rock cooling histories can be sensitive to short wavelength tectonic processes and abrupt changes of denudation rate are unlikely to be expressed in the smooth landscape evolution model presented here. Finally, fission track annealing can result in bias toward younger AFT ages, and therefore higher denudation rates, which is consistent with systematic undeprediction.

6 Discussion

6.1 Continental Epeirogeny

The stratigraphic and biostratigraphic inventories that we exploit were taken from a substantial body of published paleoaltimetric constraints. They provide excellent evidence for staged regional Cenozoic growth of North American topography, with at least 2 km of topography having been generated since Campanian times (~ 82 Ma; Figure 2; *Chamberlain et al.*, 2012). To further explore and constrain the history of vertical motions and subplate support, we solved for spatially and temporally smooth rock uplift histories by inverting a continental inventory of river profiles. This inverse model was calibrated using a small number of incision rates from the Colorado Plateau [*Karlstrom et al.*, 2008; *Roberts et al.*, 2012a]. The calculated uplift history is consistent with the independent inventory of stratigraphic and biostratigraphic uplift constraints across the Colorado-Columbia-Rocky Mountains plateaus, for large portions of the Appalachian Mountains, for Mexico and for the Gulf Coast. It is also broadly consistent with a range of other independent uplift constraints (e.g. clumped and stable isotopes, magmatism; *Fitton et al.*, 1991; *Huntington et al.*, 2010; *Chamberlain et al.*, 2012). Calculated uplift from the Rockies to Great Plains suggests that regional tilting developed during the last ~ 10 Ma, which is consistent with tilting histories recorded by the Late Miocene Ogallala Group and by the Pliocene Broadwater Formation adjacent to the North Platte river [*Duller et al.*, 2012; *Willett et al.*, 2018]. The model performs poorly where there has been significant lateral tectonic displacements (e.g. Pacific seaboard) or where spatially smooth uplift histories are less appropriate. Despite the simplicity of the inverse modeling scheme, there is a reasonable match between timing of uplift and location of paleo-shorelines inferred from the biostratigraphic inventory and from previous studies (Figure 12; *Ziegler et al.*, 1985; *Kauffman and Caldwell*, 1993; *Smith et al.*, 1994; *Roberts and Kirschbaum*, 1995).

Observed and calculated uplift rates are broadly consistent and suggest that North American topography grew in several stages. These results imply that drainage planforms tend to respond to changes in uplift rate in a predictable fashion, which can be exploited to investigate continental-scale histories of regional uplift. An important test of this approach is to compare calculated uplift and denudation with independent observations. In Figures 9 and 11, we show that a simple erosional model can yield results that provide a reasonably good match. The calibrated value of v is appropriate for extracting continental-scale uplift histories from drainage (Supporting Information). These combined results provide additional constraints for the driving mechanisms of continental epeirogeny (Figure 12).

6.2 Consequences for Landscape Evolution

The inverse modeling strategy that we have described and applied makes a series of simplifying assumptions that warrant further discussion. With regard to the drainage evo-

©2018 American Geophysical Union. All rights reserved.

Accepted Article

lution of North America, there are three significant concerns: simplicity of our erosional model, stability of the drainage planform, and the influence of glaciation.

First, we have assumed a simplified version of the non-linear stream power erosional model. This model appears to be sufficiently complex to fit large inventories of river profiles with geologically meaningful uplift rate histories in that they are comparable to independent constraints (e.g. Figure 9). This model assumes that the values of the erosional parameters, v and m, are constant and that shockwaves are unimportant at long wavelengths (i.e. n=1; Equations 2 & 8). Implicit in these assumptions is that substrate (e.g. bedrock lithology, alluvium), biota, hydrodynamic processes and changes in climate (e.g. precipitation, discharge) do not set the pace of landscape evolution at long wavelengths and timescales of tens of millions of years. More generally, poor correlations between substrate (or change in substrate) as a function of river elevation, slope, curvature or calculated stream power at wavelengths greater than a few kilometers support the suggestion that lithology may not control channel geometry at wavelengths of more than a few kilometers [*Roberts et al.*, 2012a; *Paul et al.*, 2014; *Czarnota et al.*, 2014]. These observations are consistent with spectral analyses of longitudinal river profiles, which indicate that their shapes are dominated by wavelengths > 10 km, and that river profiles from adjacent catchments contain commonalities generated by regional uplift [*Roberts et al.*, 2019; *Roberts*, 2019]. Nevertheless, there is a substantial body of work which demonstrates that at smaller scales these processes determine the efficacy of fluvial erosion and the geometry of river profiles (e.g. *Armitage et al.*, 2018; *Baynes et al.*, 2018; *Forte and Whipple*, 2018; *Gallen*, 2018). It is unclear how these complex, dynamic, threshold-dependent, and undoubtedly non-linear, processes scale over geologic timescales. However, at a continental scale, we propose that the long wavelength portions of landscapes are controlled by regional uplift but moderated by integrated fluvial erosion through time and space in a predictable way.

The way in which erosion scales with slope is debated. For example, the value of the slope exponent in the stream power model, n, might range between $2/3$ to $5/3$ or greater, and may be location, process and scale dependent (e.g. *Howard and Kerby*, 1983; *Whipple and Tucker*, 1999; *Attal et al.*, 2008; *Whittaker and Boulton*, 2012; *Lague*, 2014). If $n > 1$, then information about tectonic history may be lost from longitudinal river profiles (e.g. *Pritchard et al.*, 2009; *Royden and Perron*, 2013). However, several observations exist which suggest that the integrated history of fluvial erosion on scales of $O(10^2–10^3)$ km and $O(1–10)$ Ma may depend linearly on slope. For instance, *Czarnota et al.* [2014] shows that there is a global minimum at $n = 1$ by minimising misfit between modeled and observed longitudinal river profiles of modern and ancient thalwegs of the Tumut river, Eastern Australia. In general, testing and validation of fluvial erosional models at long wavelengths and timescales is difficult [*Salles et al.*, 2017]. Large inventories of independent constraints on surface and rock uplift can be used to evaluate the success of erosional models (see Supporting Information). The simple, linear version of the stream power erosion model we use appears to provide sufficient complexity to match observed longitudinal river profiles and reproduce meaningful uplift histories. However, we acknowledge that at short timescales and length scales, more complex erosional models might be more appropriate.

A second and related issue concerns the evolution of drainage planforms (e.g. *Willett et al.*, 2014). There is much uncertainty about the longevity of drainage networks. Changing drainage planforms by divide migration or by stream capture should, with time, rearrange catchment planforms thus rendering attempts to extract information about uplift signal problematic, especially over long temporal and spatial scales. However, a small number of observations suggest that, at large scales, the assumption of essentially fixed drainage planforms could be a reasonable one. First, laboratory sand-box experiments point to the importance of pre-existing topography in determining the fixity of drainage divides and the extent to which they can migrate under changing experimental conditions

©2018 American Geophysical Union. All rights reserved.

Accepted Article

(e.g. *Lague et al.*, 2003; *Bonnet*, 2009). We note that fluvial systems have been used to infer lateral migration of drainage divides by using simple geomorphic parameters (e.g. χ). Unfortunately, use of these simple metric values require unreasonable assumptions about the spatial pattern of uplift rate which are demonstrably incorrect, especially at continental length scales [*Herman and Braun*, 2006].

Landscape evolution models suggest that drainage divide migration is not especially significant and in any case the inverse modeling presented here is robust to large excursions in values of upstream drainage area since A is taken to a fractional power. Nonetheless, we can examine how calculated uplift histories are affected by changing drainage planform by comparing our results with the history of long-term planform evolution inferred by detrital zircon studies [*Blum and Pecha*, 2014]. In Figure 2, we summarize measurements of detrital zircon ages along the northern margin of the Gulf of Mexico. Figure 2e shows crustal and magmatic zircon source terranes adapted from Figure DR5 of *Blum and Pecha* [2014] where the cumulative percentage plots of Figure 2f were redrafted from their Figure DR6. Their observations suggest that the Paleocene drainage planform had a broadly similar distribution to that of the present day. For example, $>$ 50% of the zircons in Paleocene samples close to the eastern tributaries were derived from the Grenville (1250–950 Ma), Mid-Continent (1500–1300 Ma) and Appalachian (750–280 Ma) terranes (e.g. sample 43). Paleocene samples located west of the Mississippi river have $>$ 50% of zircons ages that correspond to the Yavapai-Mazatzal (1800–1600 Ma) and Western Cordillera (275–50 Ma) terranes (e.g. sample 64). These observations imply the large-scale planform of the Mississippi catchment may not have significantly changed during Cenozoic times.

Another way to estimate longevity of drainage patterns is to compare observed and predicted sedimentary flux. Sedimentary flux was calculated by integrating incision rate in a downstream direction using the landscape evolution model shown in Figure 10. The tectonic history of western North America complicates interpretation of sedimentary flux observations from, for example, the Los Angeles basin or Baja California (see e.g. *Dorsey et al.*, 2018). In contrast, the Gulf of Mexico appears to have acted as a stable depositional sink since Cretaceous times (*Galloway et al.*, 2000). Figure 10c–e compares predicted to independent estimates of flux in the Gulf of Mexico [*Galloway et al.*, 2011]. Calculated cumulative denudation is highest in the regions of highest predicted uplift rates (e.g. Rocky Mountains-Colorado plateaus, Appalachian Mountains, Yukon, Mexican Highlands). Predicted sedimentary flux is smoother than that measured by *Galloway et al.* [2011], which is unsurprising because the landscape model was parameterized using a damped, smooth, rock uplift history. The biggest discrepancy between predicted and observed flux is at $\sim$ 60 Ma (e.g. the Wilcox Formation). We note that model coverage in the headwaters of the Mississippi catchment is low before $\sim$ 55 Ma (Figure 10c).

Finally, we have ignored the possible effects of glacial erosion and widespread continental ice cover during the last glacial maximum, partly for simplicity but mostly because it is not obvious how this issue can be addressed in a transparent way. Most of the area that was covered by ice sheets is located within the cratonic regions of northern and eastern Canada where glacial isostatic rebound continues to be the driver of surface uplift. Temporal resolution of the inverse model presented here is too coarse to accurately compute the effect of this glacial signal. The effect that extensive ice sheets could have upon drainage planform and their efficiency in topographic erosion relative to fluvial processes are poorly understood. For example, global compilations of erosion rates from glaciers and rivers on timescales of 10^1–10^7 years implies that glacial erosion tends to decrease by one to two orders of magnitude over glacial cycles, whereas fluvial erosion rates reveal no such dependence upon time. This observation suggests that uplift histories control rates of both fluvial and glacial erosion over millennial and longer timescales [*Koppes and Montgomery*, 2009]. It remains unclear how drainage planforms were dramatically modified by the last glacial maximum ($\sim$ 21 ka; *Wickert*, 2016). Geologic constraints for the uplift

©2018 American Geophysical Union. All rights reserved.

Accepted Article

and denudation history of a region covered by the Laurentide ice sheet are sparse (Figures 2 and 4). Additional testing of the results of our inverse model for this region would be insightful.

6.3 Geodynamic Implications

Both orogenic and epeirogenic processes can generate topography. Shortening, extension, magmatic underplating and dynamic uplift all contribute toward continental uplift and, to some extent, these phenomena can be discriminated between based upon their magnitude and wavelength (e.g. *Pazzaglia and Brandon*, 1996). Cretaceous uplift of the Rocky Mountains region was partially caused by growth of Laramide-aged structures (Figures 4 and 5). The geomorphic modeling and stratigraphic observations presented here suggest that regional uplift of western North American topography has predominated. Isostatic considerations indicate that the present-day surface elevation of this extensive region is supported by density variations within and beneath the lithospheric mantle rather than by crustal thickening (e.g. *Levandowski et al.*, 2018). Rare earth element inverse modeling of $<$ 5 Ma basaltic melts with Ocean Island Basalt affinities combined with the presence of shear wave velocity anomalies constrained by earthquake tomographic models are consistent with moderately elevated mantle potential temperatures and thin ($\sim$ 70 km) lithosphere beneath western North America [*Klöcking et al.*, 2018]. These observations support the notion that large-scale dynamic topography is generated and maintained by temperature anomalies within asthenospheric mantle directly beneath a thin plate. The detailed driving mechanisms that underpin observed and predicted vertical displacements have been explored by a range of numerical flow models on different temporal and spatial scales (see, e.g., *Mitrovica et al.*, 1989; *Lithgow-Bertelloni and Gurnis*, 1997; *Liu et al.*, 2008; *Moucha et al.*, 2008; *Spasojević et al.*, 2009; *Forte et al.*, 2012; *van Wijk et al.*, 2010; *Spasojević and Gurnis*, 2012; *Rowley et al.*, 2013; *Liu*, 2014). The results from this study could provide additional constraints for such models.

7 Conclusions

Cenozoic evolution of the North American landscape is determined by combining constraints provided by stratigraphic and biostratigraphic databases with inverse and forward modeling of drainage inventories. Average uplift rates estimated from fossil and stratigraphic data suggest that, following the retreat of the Western Interior Seaway at $\sim$ 80 Ma, western North America experienced staged uplift of up to 3 km. The Yukon, Appalachian Mountains and Mexico mostly underwent Neogene uplift. By inverting 4161 longitudinal river profiles, assuming a simplified version of the widely used stream power relationship, we have generated a smooth spatio-temporal uplift history that fills the gaps between spot stratigraphic and biostratigraphic constraints. Mapped drainage planforms indicate that North American rivers flow radially from large-scale swells, which have wavelengths of the order 100–1000 km. The principal swells are centered on the Colorado-Columbia-Rocky Mountains plateaus, Yukon, Appalachians and Mexico where sub-plate dynamic support is important. Predicted regional uplift rates of the Colorado-Columbia-Rocky Mountains plateaus increased from $\sim$ 0.02 mm/a between 80 and 50 Ma to $\sim$ 0.1 mm/a between 30 and the present day. To estimate denudation and to examine sensitivities of drainage patterns to tectonic forcing, we parameterized the Badlands landscape evolution model using the inverted uplift history. The results of this forward simulation is compared with a synthesis of independent estimates of denudation from thermochronometric studies and with continent-wide provenance analyses.

Several significant implications are apparent. First, substantial compilations of stratigraphic observations can be used to gauge uplift and denudation rates at large length and timescales. Secondly, drainage patterns can be inverted by assuming a simplified version of the stream power relationship despite the apparent complexity of eroding landscapes.

©2018 American Geophysical Union. All rights reserved.

Accepted Article

This modeling approach provides a useful way to constrain uplift histories on continental scales. Finally, measured and calculated uplift and denudation histories are consistent with Cenozoic sub-plate support which seems to have played a defining role in generating the North American landscape, especially at wavelengths greater than a few tens of kilometers.

Acknowledgments

We thank E. Kite, C. O'Malley, P. Mannion, C. Pont, C. Richardson, D. Rowley, J. Rudge, S. Stephenson and A. Wickert for helpful discussion. We are grateful to S. Willett for providing a helpful and insightful review. NAVDAT database can be accessed at `www.navdat.org`, ASTER GDEM data can be downloaded from `http://gdem.ersdac.jspacesystems.or.jp`, SRTM database can be downloaded from `srtm.csi.cgair.org`, and Paleobiological database can be accessed at `https://paleobiodb.org/`. PaleoDB data was downloaded on the 25th October 2017 for Campanian, Maastrichtian and Cenozoic time intervals. Cambridge Earth Sciences contribution number esc.4514.

8 Figures

©2018 American Geophysical Union. All rights reserved.

Accepted Article

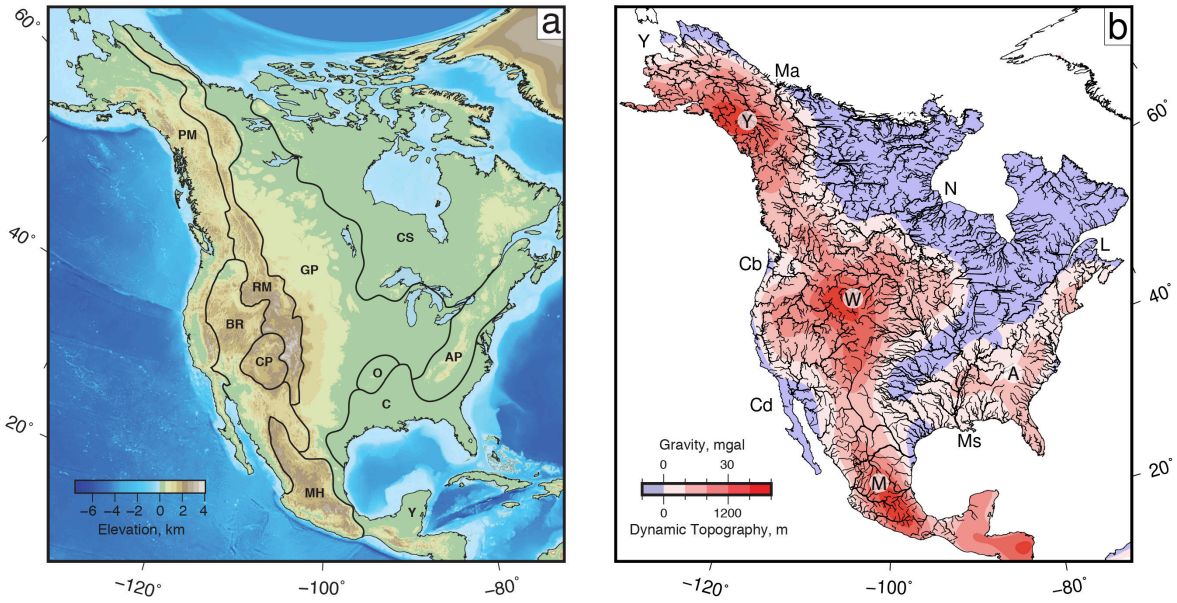
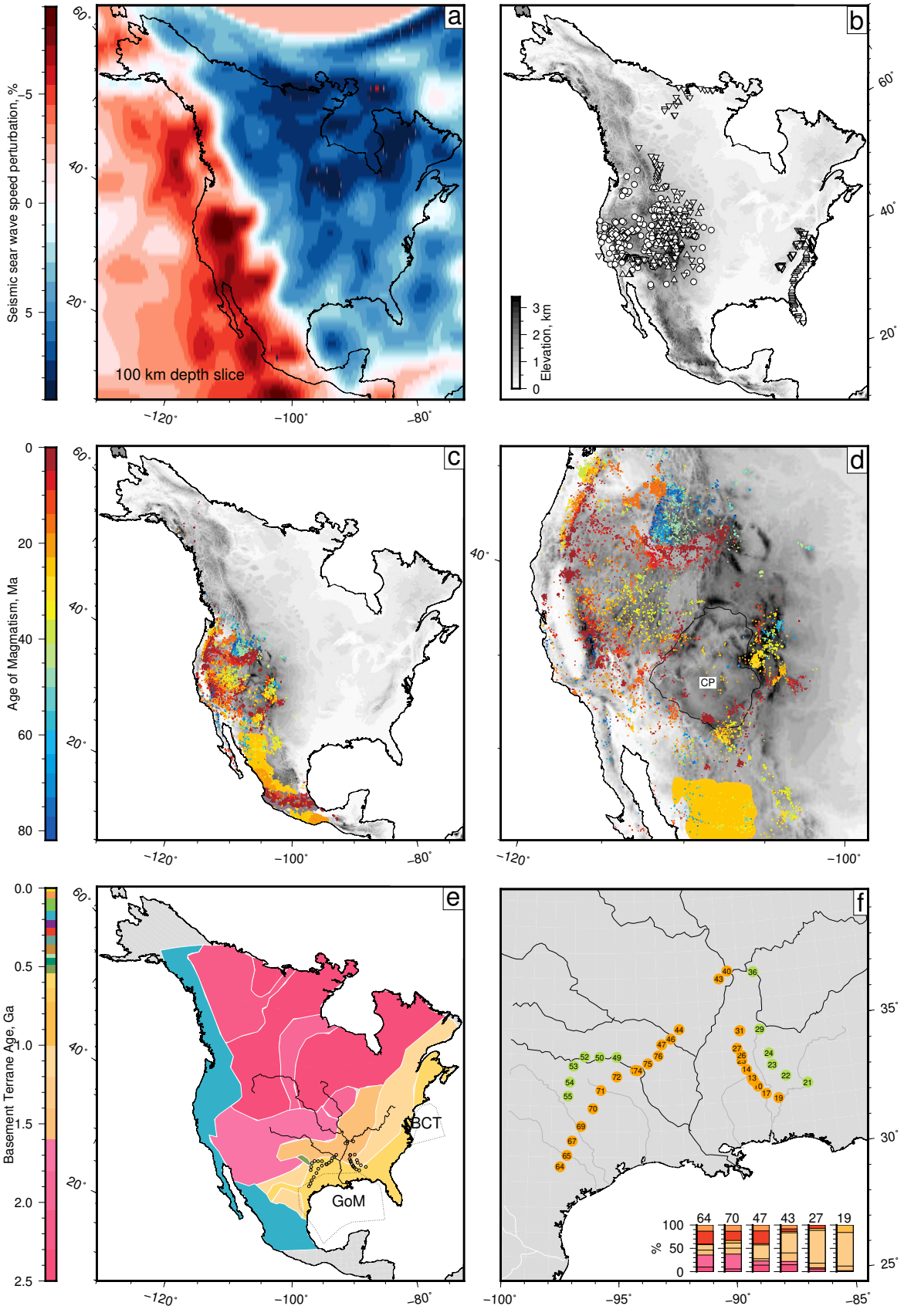


Figure 1. Topography, drainage and dynamic support of North America. (a) Topographic map based upon ETOPO1 database where physiographic provinces are named using nomenclature of *Fenneman* [1928]. PM = Pacific margin; RM = Rocky Mountains; BR = Basin and Range; CP = Colorado Plateau; GP = Great Plains; CS = Canadian Shield; O = Ozark-Ouachita Plateau; AP = Appalachian mountains; C = Gulf and Atlantic Coastal Plains; MH = Mexican Highlands. Albers Equal Area projection. (b) Thin black lines = 4161 rivers extracted from ASTER GDEM database. Ms = mouth of Mississippi; L = St. Lawrence; N = Nelson; Ma = Mackenzie; Y = Yukon; Cb = Columbia; Cd = Colorado. Drainage network is draped over dynamic topography that is calculated from long wavelength (i.e. < 800 km) free-air gravity anomalies assuming admittance, $Z = 25$ mGal/km (GRACE mission database; *Tapley et al.*, 2005; *Stephenson et al.*, 2014). Labeled circles indicate centers of major swells. Y = Yukon; W = western North America; A = Appalachians; M = Mexico.

©2018 American Geophysical Union. All rights reserved.

Accepted Article



©2018 American Geophysical Union. All rights reserved.

Accepted Article

Figure 2. Mantle velocities, uplift, magmatism and sedimentary provenance. (a) Shear wavespeed anomalies beneath North America at depth of 100 km [*Schaeffer and Lebedev*, 2013]. (b) Distribution of uplift (upward triangles), denudation (downward triangles), paleoaltimetry (circles) and paleoflow (squares) measurements since Late Cretaceous times (see text for references). (c) North American Cenozoic magmatism from NAVDAT database (*Ferrari et al.*, 2012; `www.navdat.org`). Gray shading = present-day topography from ETOPO1 database; orange/yellow polygons = Oligocene/Miocene ignimbrites [*Ferrari et al.*, 1999; *Chapin et al.*, 2004]. (d) Western North American magmatism centered on Colorado Plateau, which is outlined by black polygon labeled CP. (e) Basement terranes colored by age (after *Blum and Pecha*, 2014). Solid black lines = portion of present-day Mississippi drainage; circles = Cenomanian and Paleogene fluvial sandstones [*Blum et al.*, 2017]. Dotted polygons labelled GoM/BCT = Cenozoic clastic sedimentary deposition within Gulf of Mexico/Baltimore Canyon Trough [*Poag and Sevon*, 1989; *Galloway et al.*, 2011]. (f) Detrital zircons and drainage patterns along northern fringe of Gulf of Mexico. Black/gray/white lines = Mississippi/Texan/Mexican rivers; labeled circles = subset of detrital zircon samples extracted from Cenomanian (green) or Paleocene-Eocene (orange) fluvial deposits. Inset with labelled bars = cumulative percentages of detrital zircon populations at locations that correspond to annotated circles on map. Colored circles = zircon ages [*Blum et al.*, 2017].

©2018 American Geophysical Union. All rights reserved.

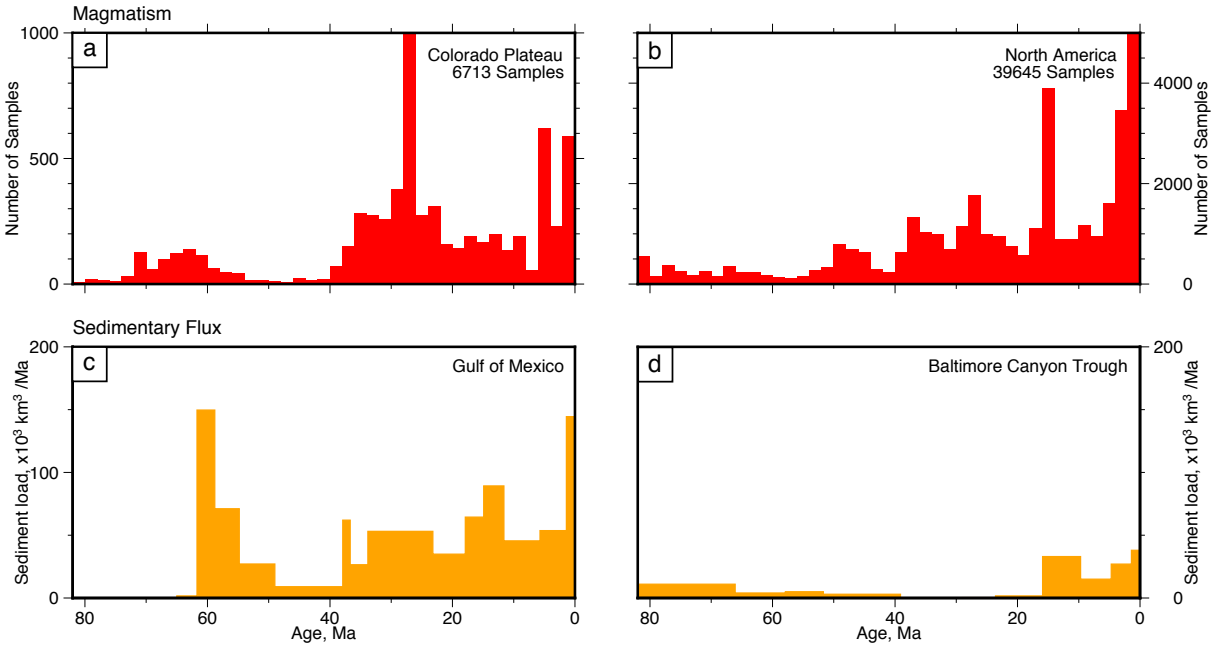
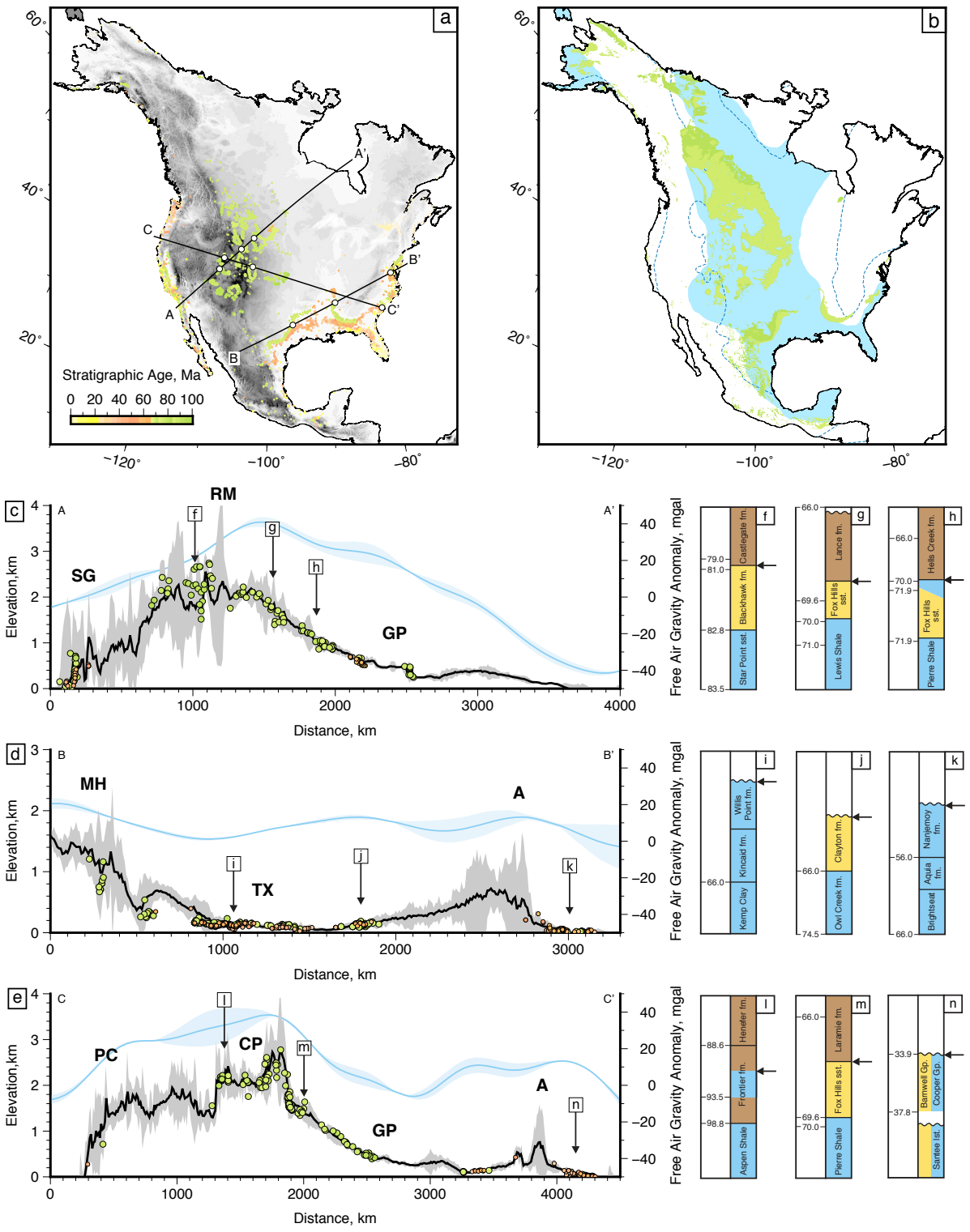


Figure 3. North American magmatism and sedimentary flux. (a) Magmatic record of Colorado Plateau taken from NAVDAT database. (b) Magmatic record of North America from NAVDAT database. (c) Solid sedimentary flux for Gulf of Mexico determined from seismic reflection surveys and well-log information by *Galloway et al.* [2011]. (d) Uncorrected sedimentary flux for New Jersey margin determined from seismic reflection surveys and well-log information by *Poag and Sevon* [1989].

©2018 American Geophysical Union. All rights reserved.

Accepted Article

Accepted Article



©2018 American Geophysical Union. All rights reserved.

Accepted Article

Figure 4. Stratigraphic and biostratigraphic constraints. (a) Colored circles show location and age of marine fossil assemblages from Paleobiology database (PBDB `paleobiodb.org`) as well as youngest marine to non-marine stratigraphic transitions [*Dickinson et al.*, 1988]. Black lines = locations of vertical cross sections shown in panels c–e; white circles = locations of stratigraphic columns shown in panels f–h, i–k and l–n. (b) Extent of Late Cretaceous seaway interpreted from PBDB. Solid blue polygons/dashed lines = maximum flooding extent of Cretaceous (i.e. Late Maastrichtian) interior seaway [*Smith et al.*, 1994; *Kauffman and Caldwell*, 1993]. Dark/light green polygons = outcropping Lower/Upper Cretaceous rocks [*Reed Jr. et al.*, 2005]. (c–e) Topographic and stratigraphic cross sections (see panel a for location); black line with gray band = topography ± maximum and minimum elevation within 100 km swath; labeled arrows = location of stratigraphic columns shown in adjacent panels; colored circles = biostratigraphically dated marine rock colored according to age (see scale bar); light blue band = free-air gravity anomaly ± maximum and minimum within 100 km swath from GRACE database (Figure1). SG = San Gabriel Mountains, RM = Rocky Mountains, GP = Great Plains, MH = Mexican Highlands, TX = Texas, A = Appalachian Highlands, PC = Pacific Coast Ranges, CP = Colorado Plateau. (f–n) Generalized stratigraphic sections with youngest marine regression or outcropping marine strata (arrow); blue boxes = shallow marine facies; yellow boxes = marginal marine/shoreface facies; brown boxes = terrestrial facies.

©2018 American Geophysical Union. All rights reserved.

Accepted Article

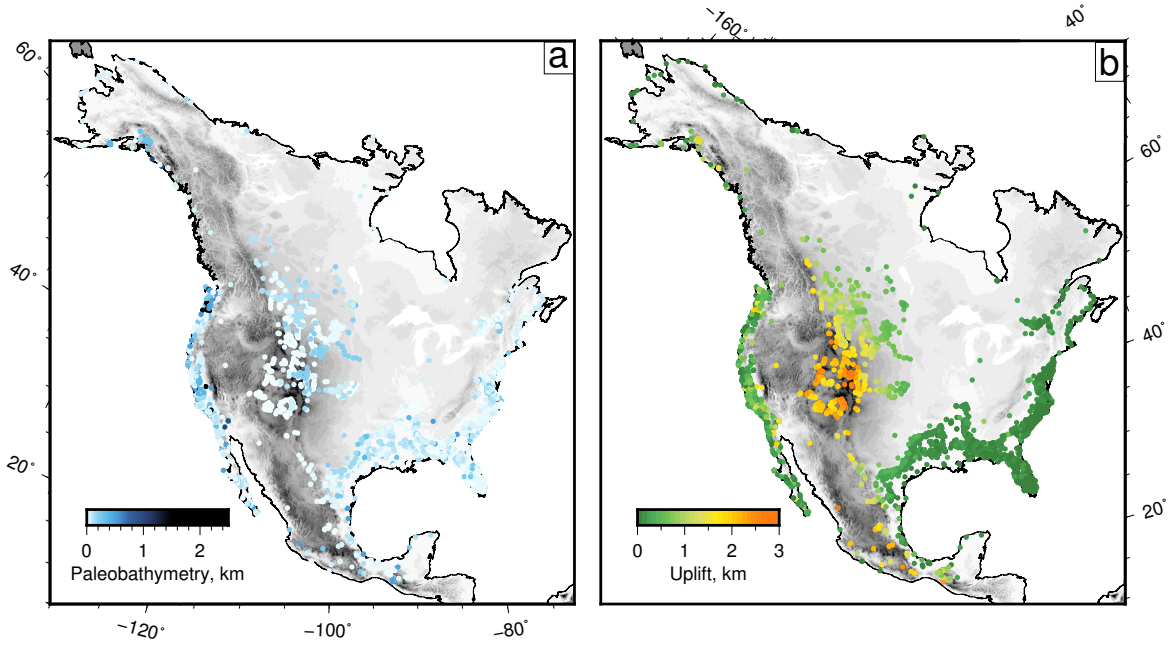


Figure 5. Paleobathymetry and cumulative uplift from stratigraphic and biostratigraphic constraints. (a) Blue circles = paleo-water depths (see scale bar). (b) Colored circles = cumulative uplift determined from marine to terrestrial transitions recorded by stratigraphic record and fossil assemblages.

©2018 American Geophysical Union. All rights reserved.

Accepted Article

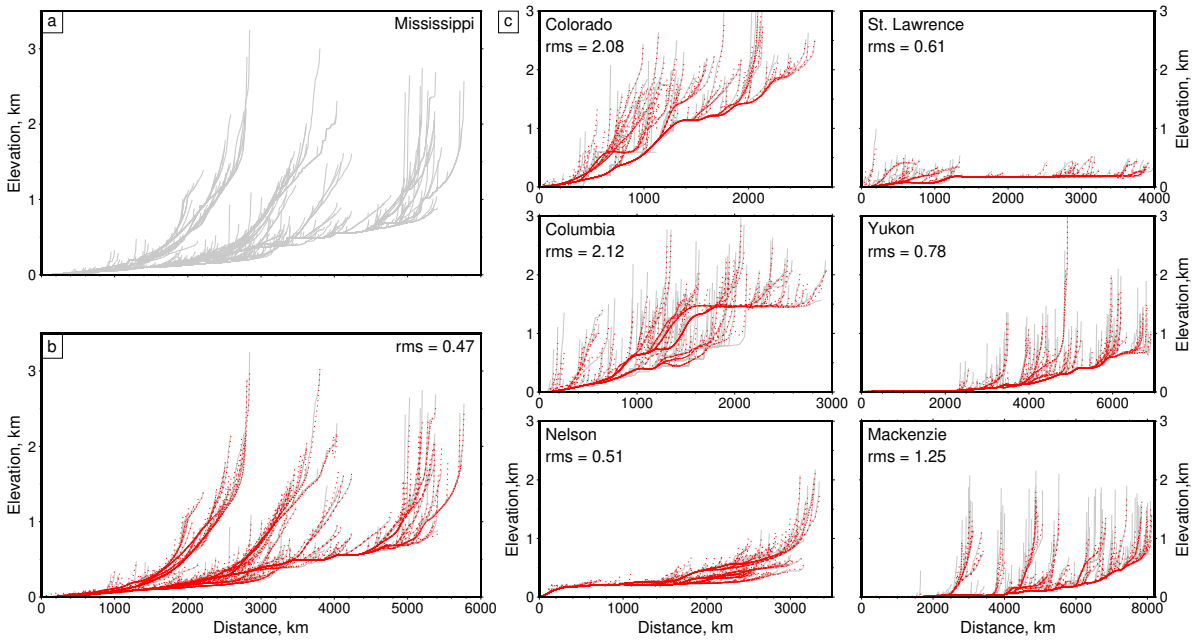


Figure 6. Inverted longitudinal river profiles. (a) Observed river profiles for Mississippi and its principal tributaries (see Figure 1). (b) Observed and calculated river profiles for Mississippi catchment. Red dotted lines = best-fitting theoretical river profiles calculated using uplift history shown in Figure 7; value of root-mean-squared (rms) misfit is shown in top right-hand corner. (c) Observed and calculated river profiles from six catchments shown in Figure 1.

©2018 American Geophysical Union. All rights reserved.

Accepted Article

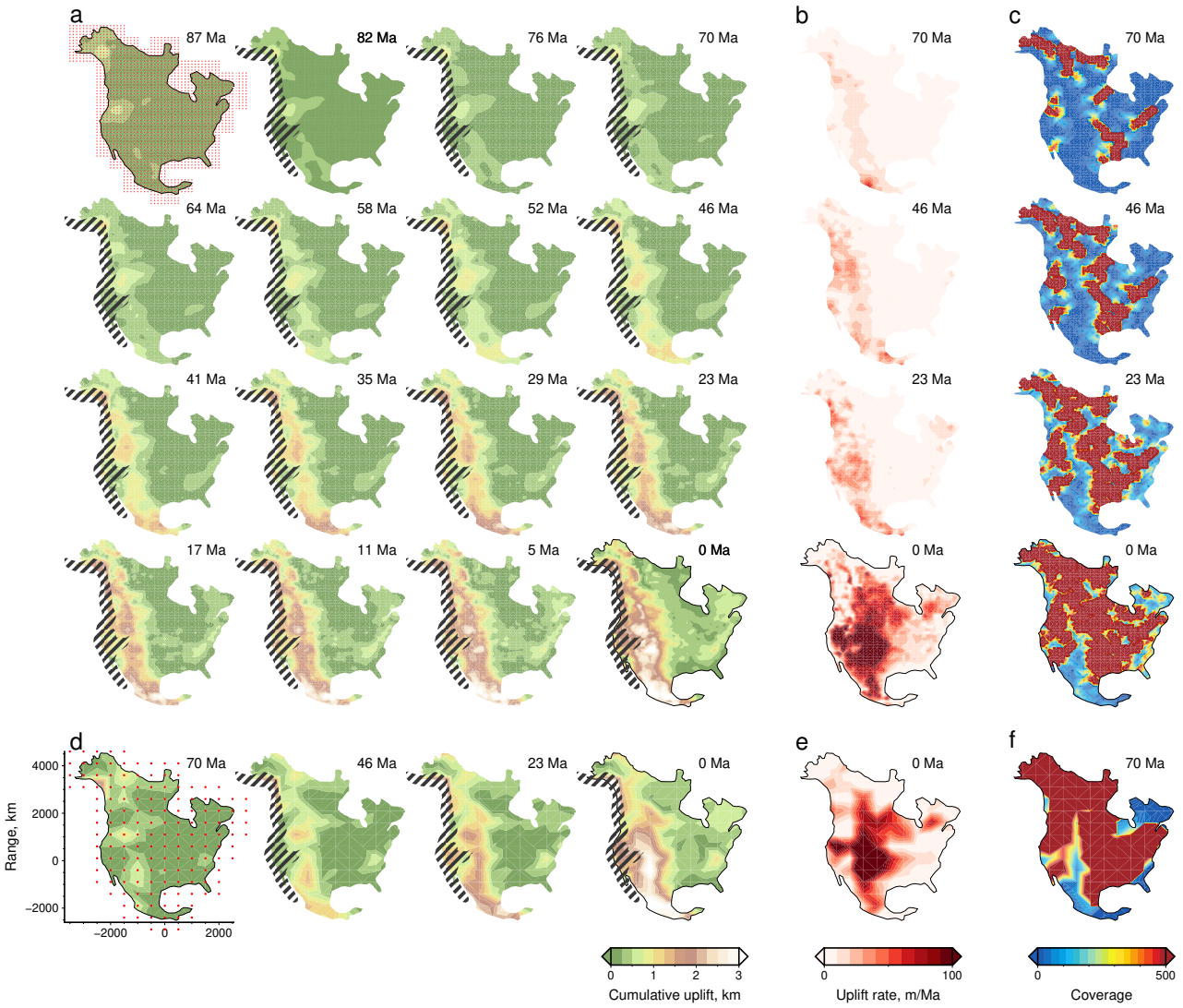


Figure 7. Calculated uplift history for North America. (a) 16 panels that show cumulative uplift history (i.e. temporally integrated uplift rate history) calculated by linear inverse modeling of 4161 river profiles (residual rms misfit = 1.25; Figure 6). Grid of red points in top left-hand panel = loci of vertices used to discretize uplift rate. Age, in millions of years, is shown for each panel. Hatched region = Great Basin and Pacific margin where internal drainage, plate accretion and strike-slip tectonics compromise assumptions that underpin inverse model. (b) Calculated uplift rate at four different times. (c) Selected panels at four different times that show model coverage (i.e. number of non-zero entries in model matrix, M, corresponding to given uplift node). Note that model coverage is highest toward present day and significantly decreases for ages > 70 Ma (see Figure 8c). (d) Four panels showing cumulative uplift history of North America calculated using coarser mesh (residual rms misfit = 2.62). (e) and (f) Calculate uplift rates and model coverage for coarser mesh at 0 Ma.

©2018 American Geophysical Union. All rights reserved.

Accepted Article

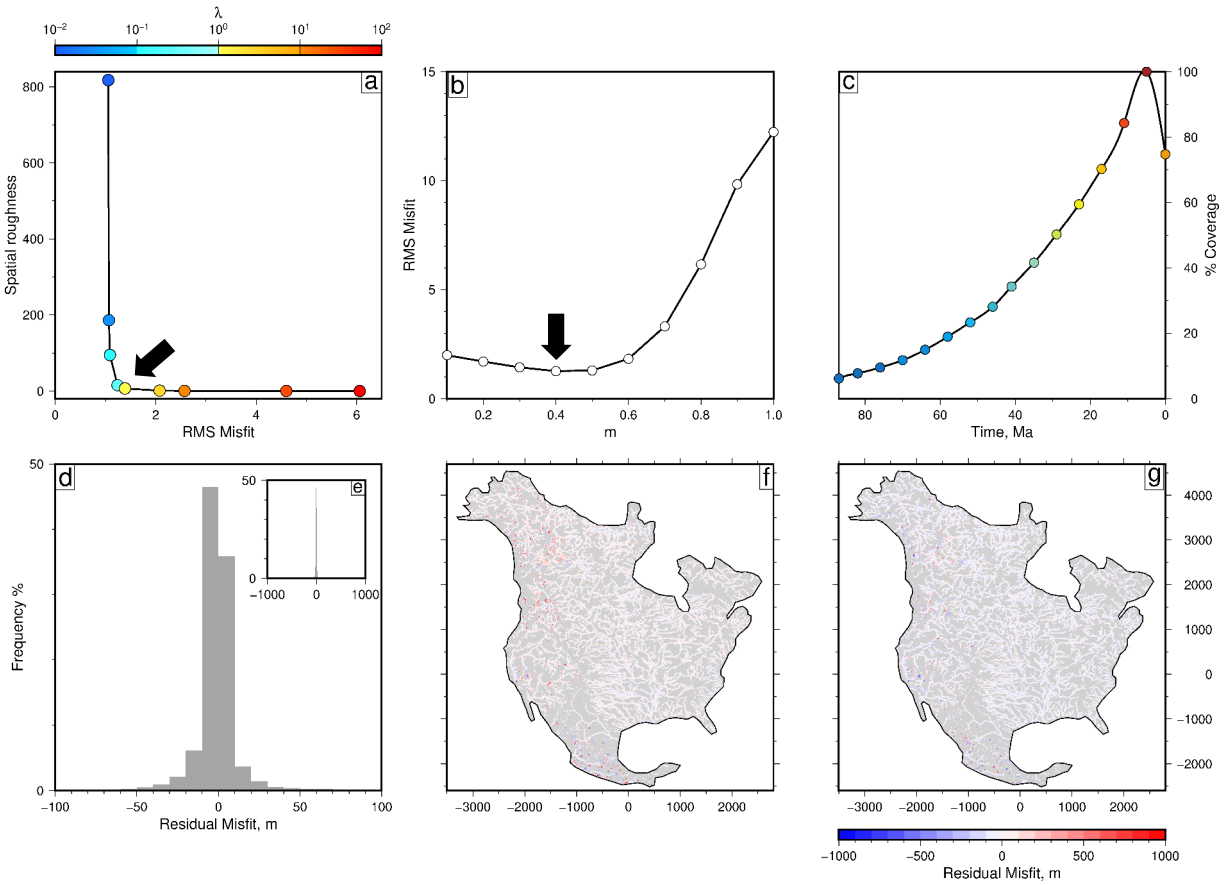


Figure 8. Inverse model parametrization. (a) Data misfit plotted as function of model smoothness for suite of inverse models with different values of smoothing parameter, λ_S (see Figure 7a for configuration of inverse model). Black arrow = locus of smoothest, best-fitting model where λ_S = 0.5. (b) Residual misfit plotted as function of erosional parameter m. Black arrow = locus of weak global minimum at $m \approx 0.4$. (c) Cumulative model coverage as a function of time (Figure 7c). (d) Histogram of residual misfit between observed and predicted river profiles. (e) Inset showing full frequency distribution of residuals. (f) Residual positive misfit map between observed and calculated river profiles. (g) Residual negative misfit map.

©2018 American Geophysical Union. All rights reserved.

Accepted Article

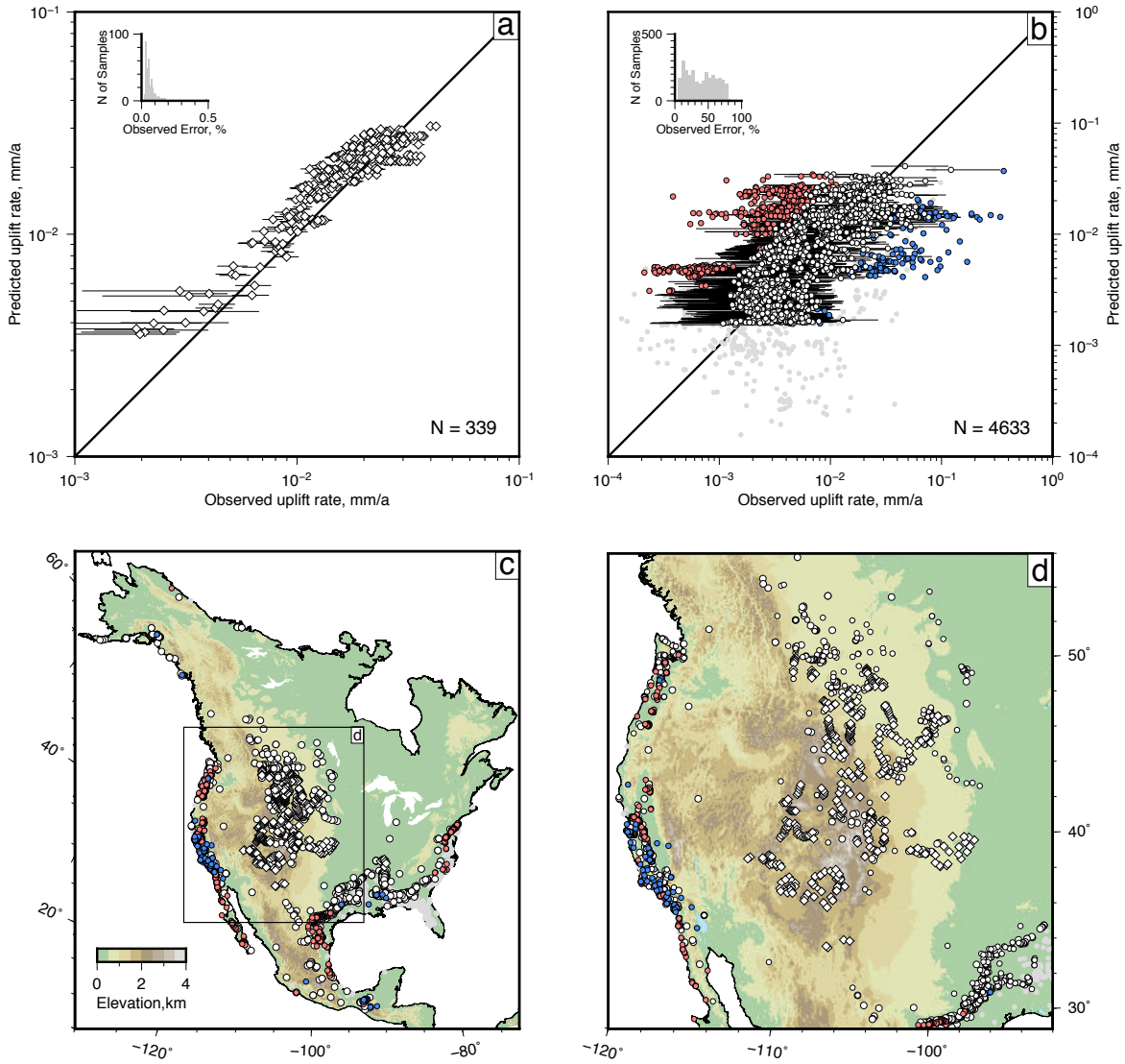
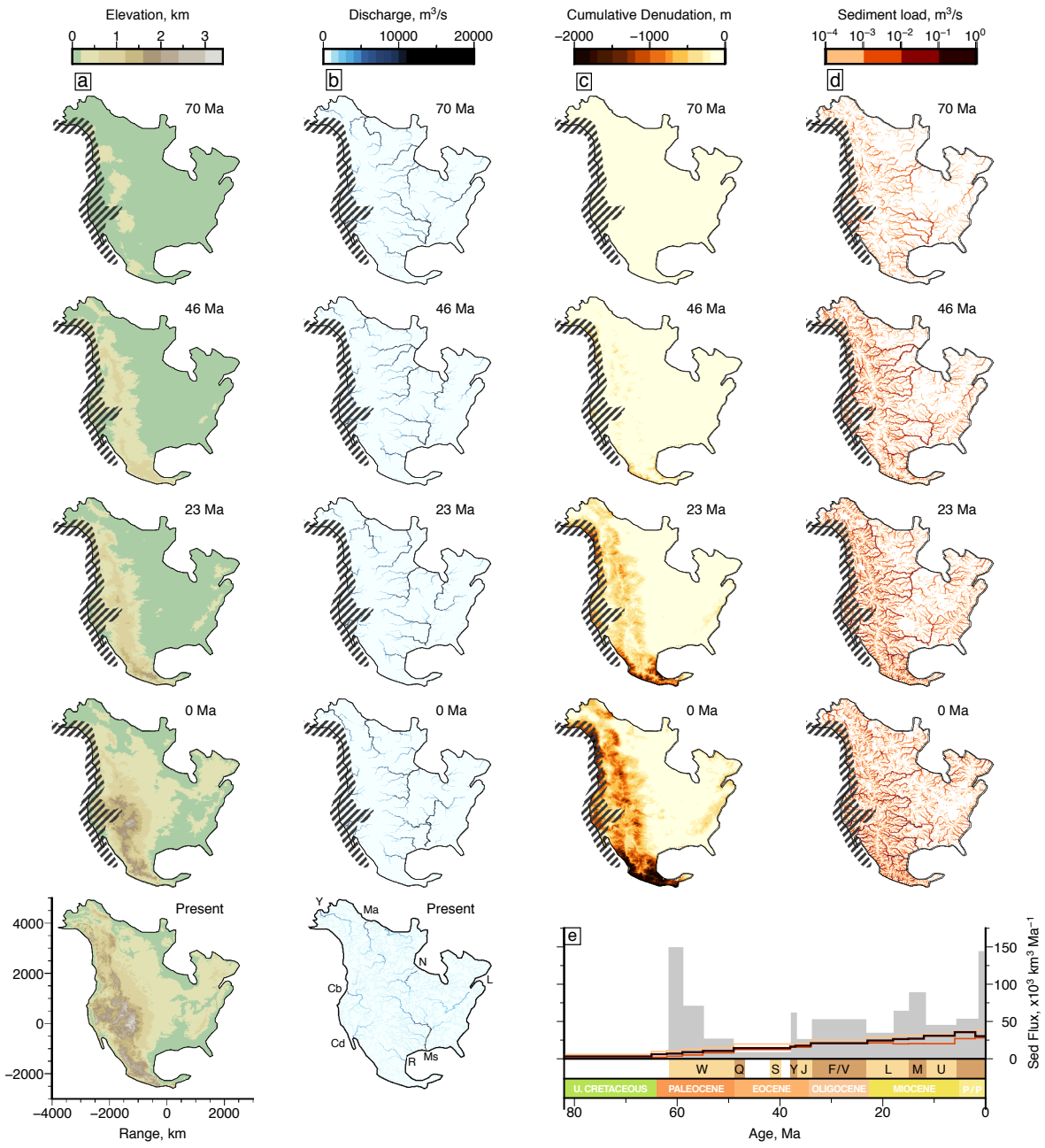


Figure 9. Testing results of inverse modeling. Comparison of time-averaged Late Cretaceous to Recent uplift from inverse model and (a) stratigraphic and (b) biostratigraphic constraints (Figures 4f-n and 4a, respectively). Inset histograms = percentage error distribution of observations. Solid black line = 1:1 relationship; white circles = inverse results that agree with stratigraphic estimates; gray points = samples with large observational uncertainties (i.e. greater than one order of magnitude) with error bars omitted for clarity; red/blue points indicate where inverse model over-/under-predicts uplift rate by more than a factor of two. (c) Spatial distribution of stratigraphic and biostratigraphic constraints colored by accuracy of inverse model. Symbols same as for panels a and b. (d) Comparison of inverse modeling results and observations centered on Colorado Plateau (labelled box in panel c). Inverse model best matches uplift measurements across the Colorado Plateau and Rocky Mountains. Supporting Information shows results obtained when erosional parameter, v, is increased/decreased by one order of magnitude.

©2018 American Geophysical Union. All rights reserved.

Accepted Article



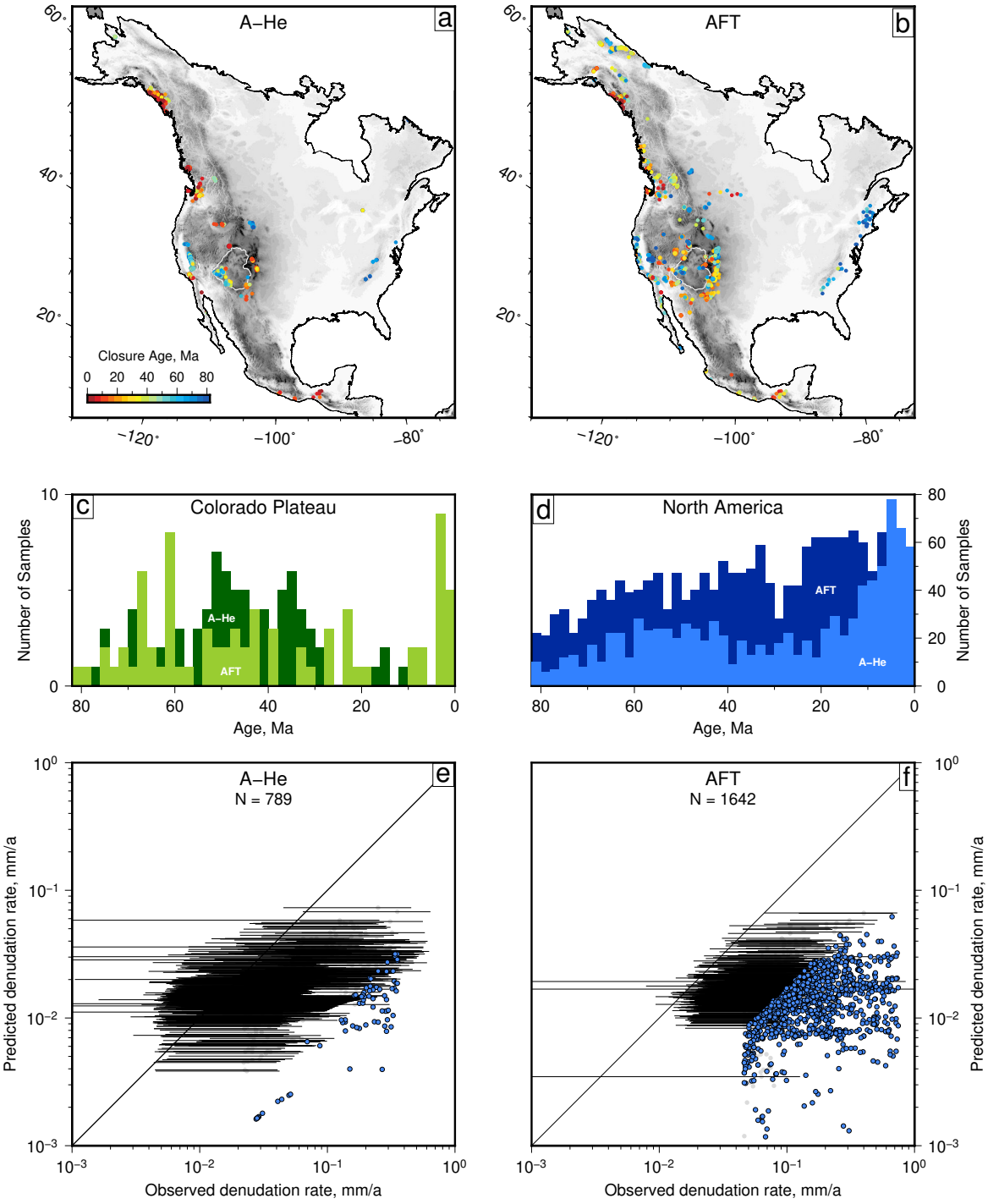
©2018 American Geophysical Union. All rights reserved.

Accepted Article

Figure 10. Predicted landscape evolution. (a) Late Mesozoic and Cenozoic topographic evolution of North America calculated using modified version of Badlands landscape evolution model [*Salles*, 2015]. Model was forced using uplift history calculated by inverse modeling (Figure 7). Model resolution = 10 km. Hatched region = portion of model where calculated uplift history should be treated with caution. Lowest panel = present-day topography from ASTER GDEM database for comparison. (b) Calculated discharge. Bottom panel = present-day discharge calculated using Esri flow-routing algorithms and ASTER GDEM database (see Figure 1 for annotation. (c) Calculated cumulative denudation (i.e. $\int \partial z \mathrm{dt}/\partial \mathrm{t}$). (d) Calculated sedimentary load (i.e. $\int \partial z \mathrm{dx}/\partial \mathrm{t}$). (e) Gray histogram = observed solid sedimentary flux for Gulf of Mexico redrawn from *Galloway et al.* [2011]. Orange/black/red lines = flux calculated for three different Badlands landscape evolution models parameterised using 1, 5 and 10% starting conditions (see Supporting Information). Brown/peach band shows stratigraphy: W = Wilcox; Q = Queen City; S = Sparta; Y = Yegua; J = Jackson; F/V = Frio/Vicksburg; L, M, U = Lower, Middle and Upper Miocene. Note model coverage is $<$ 20% before 55 Ma (see Figure 8c).

©2018 American Geophysical Union. All rights reserved.

Accepted Article



©2018 American Geophysical Union. All rights reserved.

Accepted Article

Figure 11. Comparison of thermochronmetric and calculated denudation rates. (a) Synthesis of independent estimates of U-Th/He (A-He) closure ages for North America. Gray shading = present-day topography calculated from ETOPO1 database; thin white line encloses Colorado Plateau. (b) Apatite Fission Track (AFT) closure ages. (c) Histograms of A-He and AFT closure ages from Colorado Plateau. (d) Histograms of closure ages for North America. (e) Comparison of denudation rates calculated from landscape evolution model that was parameterized using results of inverse modeling (Figure 10c) and independent A-He closure ages (see panels a and b). Error bars = data where match between the parametrized forward model and independent estimates is good; blue points = data where calculated denudation rates are factor of two or more lower than A-He estimates where error bars have been omitted for clarity (see Supporting Information). (f) Comparison of calculated denudation rates and independent estimates from AFT closure ages.

©2018 American Geophysical Union. All rights reserved.

Accepted Article

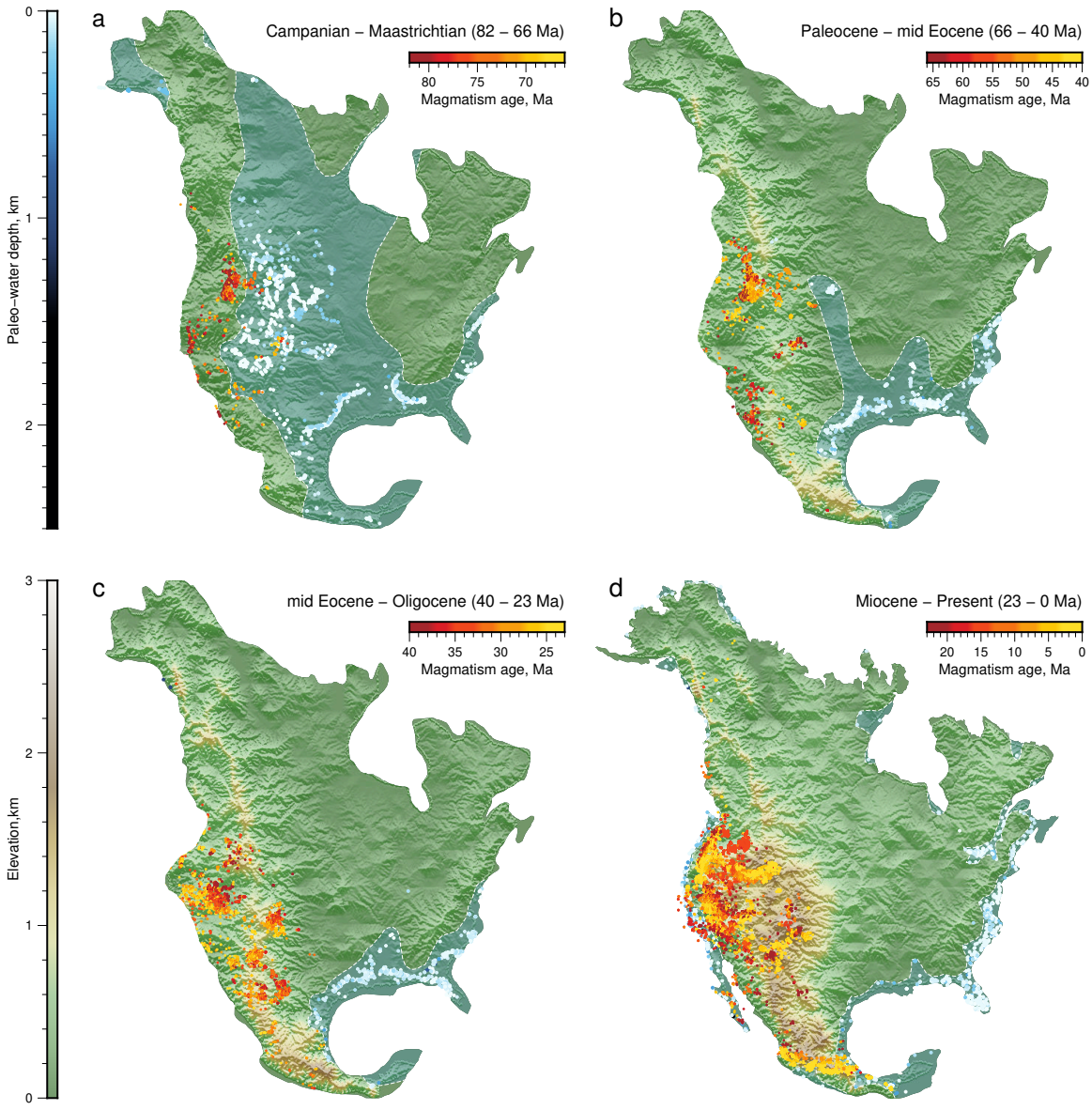


Figure 12. Landscape evolution model of North America. Four panels show calculated Mesozoic to Cenozoic topographic evolution compared with coeval independent paleogeographic constraints. Red circles = magmatic record from NAVDAT database (Figure 2); blue circles = stratigraphic shoreline markers/marine fossils from PBDB (Figure 4); light blue shading = maximum flooded surface from *Smith et al.* [1994] revised with stratigraphic and biostratigraphic constraints presented here.

©2018 American Geophysical Union. All rights reserved.

Accepted Article

References

Ainsworth, N. R., L. Riley, H. W. Bailey, and K. J. Gueinn (2014), Cretaceous–Tertiary stratigraphy of the Labrador Shelf, *Riley Geoscience Ltd.*, commissioned by Nalcor Energy, http://www.nalcorenergy.com/ OILGAS/labrador-biostratigraphy.asp

Allen, G. H., J. B. Barnes, T. M. Pavelsky, and E. Kirby (2013), Lithologic and tectonic controls on bedrock channel form at the northwest Himalayan front, *J. Geophys. Res. Earth Surf.*, *118*(3), 1806–1825, doi:10.1002/jgrf.20113.

Amidon, W. H., M. Roden-Tice, A. J. Anderson, R. E. McKeon, and D. L. Shuster (2016), Late Cretaceous unroofing of the White Mountains, New Hampshire, USA: An episode of passive margin rejuvenation?, *Geology*, *44*(6), 415–418, doi:10.1130/G37429.1.

Anderson, R. S., and S. P. Anderson (2010), *Geomorphology: the mechanics and chemistry of landscapes*, Cambridge University Press.

Armitage, J. J., and P. A. Allen (2010), Cratonic basins and the long-term subsidence history of continental interiors, *J. Geol. Soc. London.*, *167*(1), 61–70, doi:10.1144/0016-76492009-108.

Armitage, J. J., A. C. Whittaker, M. Zakari and B. Campforts (2018), Numerical modelling of landscape and sediment flux response to precipitation rate change, *Earth Surf. Dyn.*, *6*, 77–99.

Arthur, M. A., and B. B. Sageman (2004), Sea-level control on source-rock development: Perspectives from the Holocene Black Sea, the Mid-Cretaceous Western Interior Basin of North America, and the Late Devonian Appalachian Basin, *SEPM Spec. Publ.*, *82*, 35–59.

Attal, M., G. E. Tucker, A. C. Whittaker, P. A. Cowie and G. P. Roberts (2008), Modelling fluvial incision and transient landscape evolution: Influence of dynamic channel adjustment, *J. Geophys. Res. Earth Surf.*, *113*, 1–16.

Ault, A. K., R. M. Flowers, and S. A. Bowring (2013), Phanerozoic surface history of the Slave craton, *Tectonics*, *32*(5), 1066–1083, doi:10.1002/tect.20069.

Awater, T. (1970), Implications of plate tectonics for the Cenozoic tectonic evolution of Western North America, *Geol. Soc. Am. Bull.*, *81*, 3513–3536.

Baldwin, J. A., K. X. Whipple, and G. E. Tucker (2003), Implications of the shear stress river incision model for the timescale of postorogenic decay of topography, *J. Geophys. Res. Solid Earth*, *108*(B3), doi:10.1029/2001JB000550.

Barnett-Moore, N., N. Flament, C. Heine, N. Butterworth, and R. D. Müller (2014), Cenozoic uplift of south Western Australia as constrained by river profiles, *Tectonophysics*, *622*, 186–197, doi:10.1016/j.tecto.2014.03.010.

Bartow, J. A. (1991), Cenozoic evolution of the San Joaquin Valley, California, *U.S. Geol. Surv. Prof. Pap.*, *1501*, 1–40.

Baynes, E., D. Lague, M. Attal, A. Gangloff, L. A. Kirstein, and A. J. Dugmore (2018), River self-organisation inhibits discharge control on waterfall Migration, *Sci. Rep.*, *8*, 1–8, doi:10.1038/s41598-018-20767-6.

Becker, T. W., C. Faccenna, E. D. Humphreys, A. R. Lowry, and M. S. Miller (2014), Static and dynamic support of western United States topography, *Earth Planet. Sci. Lett.*, *402*(C), 234–246, doi:10.1016/j.epsl.2013.10.012.

Best, M. G., D. L. Barr, E. H. Christiansen, S. Gromme, A. L. Deino, and D. G. Tingey (2009), The Great Basin Altiplano during the middle Cenozoic ignimbrite flareup: Insights from volcanic rocks, *Int. Geol. Rev.*, *51*(7-8), 589–633, doi:10.1080/00206810902867690.

Blum, M., and M. Pecha (2014), Mid-Cretaceous to Paleocene North American drainage reorganization from detrital zircons, *Geology*, *42*(7), 607–610, doi:10.1130/G35513.1.

Blum, M. D., K. T. Milliken, M. A. Pecha, J. W. Snedden, B. C. Frederick, and W. E. Galloway (2017), Detrital-zircon records of Cenomanian, Paleocene, and Oligocene Gulf of Mexico drainage integration and sediment routing: Implications for scales of basin-floor fans, *Geosphere*, *13*(6), 2169–2205, doi:10.1130/GES01410.1.

©2018 American Geophysical Union. All rights reserved.

Accepted Article

Boettcher, S. S., and K. L. Milliken (1994), Mesozoic-Cenozoic Unroofing of the Southern Appalachian Basin: Apatite Fission Track Evidence from Middle Pennsylvanian Sandstones, *J. Geol.*, *102*(6), 655–668, doi:10.1086/629710.

Bond, G. (1976), Evidence for continental subsidence in North America during the Late Cretaceous global submergence, *Geology*, *4*, 557–560.

Bonnet, S. (2009), Shrinking and splitting of drainage basins in orogenic landscapes from the migration of themain drainage divide, *Nat. Geosci.*, *2*(11), 766–771, doi:10.1038/ngeo666.

Braun, J. (2002), Quantifying the effect of recent relief changes on age-elevation relationships, *Earth Planet. Sci. Lett.*, *200*, 331–343.

Brocard, G. Y., and P. Van Der Beek (2006), Influence of incision rate, rock strength, and bedload supply on bedrock river gradients and valley-flat widths: Field-based evidence and calibrations from western Alpine rivers (southeast France), *Geol. Soc. Am. Spec. Pap.*, *398*(07), 101–126, doi:10.1130/2006.2398(07).

Brocard, G. Y., J. K. Willenbring, T. E. Miller, and F. N. Scatena (2016), Relict landscape resistance to dissection by upstream migrating knickpoints, *J. Geophys. Res. Earth Surf.*, *121*(6), 1182–1203, doi:10.1002/2015JF003678.

Bustin, R. M. (1991), Organic maturity in the western Canada sedimentary basin, *Intl. J. Coal Geo.*, *19*, 319–358.

Campforts, B., and G. Grovers (2015), Keeping the edge: A numerical method that avoids knickpoint smearing when solving the stream power law, *J. Geophys. Res. Earth Surf.*, *120*, 1189–1205, doi:10.1002/2015JF003602.Received.

Cao, W., S. Zahirovic, N. Flament, S. Williams, J. Golonka, and R. Dietmar Müller (2017), Improving global paleogeography since the late Paleozoic using paleobiology, *Biogeosciences*, *14*(23), 5425–5439, doi:10.5194/bg-14-5425-2017.

Cassel, E. J., A. T. Calvert, and S. A. Graham (2009), Age, geochemical composition, and distribution of Oligocene ignimbrites in the northern Sierra Nevada, California: Implications for landscape morphology, elevation, and drainage divide geography of the Nevadaplano, *Int. Geol. Rev.*, *51*(7-8), 723–742, doi:10.1080/00206810902880370.

Castelltort, S., A. C. Whittaker, and J. Vergés (2015), Tectonics, sedimentation and surface processes: From the erosional engine to basin deposition, *Earth Surf. Process. Landforms*, *40*(13), 1839–1846, doi:10.1002/esp.3769.

Cather, S. M., S. D. Connell, R. M. Chamberlin, W. C. McIntosh, G. E. Jones, A. R. Potochnik, S. G. Lucas, and P. S. Johnson (2008), The Chuska erg: Paleogeomorphic and paleoclimatic implications of an Oligocene sand sea on the Colorado Plateau, *GSA Bull.*, *120*(1-2), 13–33.

Chamberlain, C. P., H. T. Mix, A. Mulch, M. T. Hren, M. L. Kent-Corson, S. J. Davis, T. W. Horton, and S. A. Graham (2012), The Cenozoic climatic and topographic evolution of the western north American Cordillera, *Am. J. Sci.*, *312*(2), 213–262, doi:10.2475/02.2012.05.

Channer, M. A., J. W. Ricketts, M. Zimmerer, M. Heizler, and K. E. Karlstrom (2015), Surface uplift above the Jemez mantle anomaly in the past 4 Ma based on $^{40}Ar/^{39}Ar$ dated paleoprofiles of the Rio San Jose, New Mexico, USA, *Geosphere*, *11*(5), 1384–1400, doi:10.1130/GES01145.1.

Chapin, C. E., M. Wilks, and W. C. Mcintosh (2004), Space–time patterns of Late Cretaceous to present magmatism in New Mexico – comparison with Andean volcanism and potential for future volcanism, *New Mex. Bur. Geol. Miner. Resour. Bull.*, *160*, 13–40.

Colgan, J. P., and C. D. Henry (2009), Rapid middle Miocene collapse of the Mesozoic orogenic plateau in north-central Nevada, *Int. Geol. Rev.*, *51*(9-11), 920–961, doi:10.1080/00206810903056731.

Croissant, T., and J. Braun (2014), Constraining the stream power law: A novel approach combining a landscape evolution model and an inversion method, *Earth Surf. Dyn.*, *2*, 155–166

©2018 American Geophysical Union. All rights reserved.

Accepted Article

Crosby, B. T., and K. X. Whipple (2006), Knickpoint initiation and distribution within fluvial networks, 236 waterfalls in the Waipaoa River, North Island, New Zealand, *Geomorphology*, *82*, 16–38, doi:10.1016/j.geomorph.2005.08.023.

Cross, T. A. (1986), Tectonic Controls of Foreland Basin Subsidence and Laramide Style Deformation, Western United States, doi:10.1002/9781444303810.ch1.

Cross, T. A., and R. H. Pilger (1978), Tectonic controls of late Cretaceous sedimentation, western interior, USA, *Nature*, *274*, 653–657.

Czarnota, K., G. G. Roberts, N. J. White, and S. Fishwick (2014), Spatial and temporal patterns of Australian dynamic topography from river profile modeling, *J. Geophys. Res. Solid Earth*, *119*(2), 1384–1424, doi:10.1002/2013JB010436.

Dávila, F. M., and C. Lithgow-Bertelloni (2015), Dynamic uplift during slab flattening, *Earth Planet. Sci. Lett.*, *425*, 34–43, doi:10.1016/j.epsl.2015.05.026.

Davis, W. M. (1899), The Geographical Cycle, *Geogr. J.*, *14*(5), 481–504, doi:10.1086/521238.

DeCelles, P. G. (1994), Late Cretaceous-Paleocene synorogenic sedimentation and kinematic history of the Sevier thrust belt, northeast Utah and southwest Wyoming, *GSA Bull.*, *106*(1), 32–56.

DeCelles, P. G. (2004), Late Jurassic to Eocene evolution of the Cordilleran thrust belt and foreland basin system, Western U.S.A., *Am. J. Sci.*, *304*(February), 105–168, doi:10.2475/ajs.304.2.105.

DiBiase, R. A., K. X. Whipple, M. P. Lamb, and A. M. Heimsath (2014), The role of waterfalls and knickzones in controlling the style and pace of landscape adjustment in the western San Gabriel Mountains, California, *Bull. Geol. Soc. Am.*, *127*(3-4), 539–559, doi:10.1130/B31113.1.

Dickie, K., C. E. Keen, G. L. Williams, and S. A. Dehler (2011), Tectonostratigraphic evolution of the Labrador margin, Atlantic Canada, *Mar. Pet. Geol.*, *28*, 1663–1675, doi:10.1016/j.marpetgeo.2011.05.009.

Dickinson, W. R., and W. S. Snyder (1978), Plate tectonics of the Laramide orogeny, in *Laramide Fold. Assoc. with Basement Block Faulting West. United States*, edited by I. I. I. Matthews Vincent, Geological Society of America.

Dickinson, W. R., M. A. Klute, M. J. Hayes, S. U. Janecke, E. R. Lundin, M. A. Mckittrick, and M. D. Olivares (1988), Paleogeographic and paleotectonic setting of Laramide sedimentary basins in the central Rocky Mountain region, *Bull. Geol. Soc. Am.*, *100*(7), 1023–1039, doi:10.1130/0016-7606(1988)100<1023:PAPSOL>2.3.CO;2.

Dickinson, W. R. (2004), Evolution of the North American Cordillera, *Ann. Rev. Earth Plan. Sci.*, *32*(1), 13–45, doi:10.1146/annurev.earth.32.101802.120257.

Dodson, M. H. (1973), Closure temperatures in cooling geological and petrological systems, *Contrib. to Mineral. Petrol.*, *40*, 259–274.

Dorsey, R. J., B. O'Connell, K. McDougall, and M. B. Homan (2018), Punctuated sediment discharge during Early Pliocene birth of the Colorado River: Evidence from regional stratigraphy, sedimentology, and paleontology, *Sediment. Geol.*, *363*, 1–33, doi:10.1016/j.sedgeo.2017.09.018.

Duller, R. A., A. C. Whittaker, J. B. Swinehart, J. J. Armitage, H. D. Sinclair, A. Bair, and P. A. Allen (2012), Abrupt landscape change post-6 Ma on the central Great Plains, USA, *Geology*, *40*(10), 871–874, doi:10.1130/G32919.1.

Elston, D. P., and R. A. Young (1991), Cretaceous-Eocene (Laramide) landscape development and Oligocene-Pliocene drainage reorganization of Transition Zone and Colorado Plateau, Arizona, *J. Geophys. Res.*, *96*(B7), 12,389–12,406, doi:10.1029/90JB01978.

Epis, R. C., and C. E. Chapin (1975), Geomorphic and tectonic implications of the Post-Laramide, Late Eocene erosion surface in the southern Rocky Mountains, in *Cenozoic Hist. South. Rocky Mt.*, edited by B. F. Curtis, pp. 45–74, Geological Society of America Memoir 144, Socorro, NM.

Fan, M., and B. Carrapa (2014), Late Cretaceous-early Eocene Laramide uplift, exhumation, and basin subsidence in Wyoming: Crustal responses to flat slab subduction, *Tec-*

©2018 American Geophysical Union. All rights reserved.

Accepted Article

tonics, *33*(4), 509–529, doi:10.1002/2012TC003221.

Farley, K. A. (2002), (U-Th)/He Dating: Techniques, Calibrations, and Applications, *Rev. Mineral. Geochemistry*, *47*(1), 819–844.

Feng, J., R. T. Buffler, and M. A. Kominz (1994), Laramide orogenic influence on late Mesozoic-Cenozoic subsidence history, western deep Gulf of Mexico basin, *Geology*, *22*(4), 359–362.

Fenneman, N. (1928), Physiographic Divisions of the United States, *Ann. Ass. Am. Geog.*, *18*(4), 261-353.

Ferrari, L., and S. Bryan (2007), Magmatism and tectonics of the Sierra Madre Occidental and its relation with the evolution of the western margin of North America, *Geol. Soc. Am.*, *2422*(01), 1–39, doi:10.1130/2007.2422(01).

Ferrari, L., M. López-Martínez, G. Aguirre-Díaz, and G. Carrasco-Núñez (1999), Space-time patterns of Cenozoic arc volcanism in central Mexico: From the Sierra Madre Occidental to the Mexican Volcanic Belt, *Geology*, *27*(4), 303–306.

Ferrari, L., M. López-Martínez, and J. Rosas-Elguera (2002), Ignimbrite flare-up and deformation in the southern Sierra Madre Occidental, western Mexico: Implications for the late subduction history of the Farallon plate, *Tectonics*, *21*(4), 1–25, doi:10.1029/2001TC001302.

Ferrari, L., T. Orozco-Esquivel, V. Manea, and M. Manea (2012), The dynamic history of the Trans-Mexican Volcanic Belt and the Mexico subduction zone, *Tectonophysics*, *522-523*(April), 122–149, doi:10.1016/j.tecto.2011.09.018.

Fitton, J. G., D. James, and W. P. Leeman (1991), Basic magmatism associated with Late Cenozoic extension in the western United States: Compositional variations in space and time, *J. Geophys. Res.*, *96*(B8), 13,693, doi:10.1029/91JB00372.

Flament, N., M. Gurnis, R. D. Müller, D. J. Bower, and L. Husson (2015), Influence of subduction history on South American topography, *Earth Planet. Sci. Lett.*, *430*, 9–18, doi:10.1016/j.epsl.2015.08.006.

Flowers, R. M., and K. A. Farley (2012), Apatite 4He/3He and (U-Th)/He Evidence for an Ancient Grand Canyon, *Science*, *338*, 1616–1619, doi:10.1126/science.1229390.

Flowers, R. M., B. P. Wernicke, and K. A. Farley (2008), Unroofing, incision, and uplift history of the southwestern Colorado Plateau from apatite (U-Th)/He thermochronometry, *Bull. Geol. Soc. Am.*, *120*(5-6), 571–587, doi:10.1130/B26231.1.

Flowers, R. M., A. K. Ault, S. A. Kelley, N. Zhang, and S. Zhong (2012), Epeirogeny or eustasy? Paleozoic-Mesozoic vertical motion of the North American continental interior from thermochronometry and implications for mantle dynamics, *Earth Planet. Sci. Lett.*, *317-318*, 436–445, doi:10.1016/j.epsl.2011.11.015.

Forte, A. M. and K. X. Whipple (2018), Criteria and tools for determining drainage divide stability, *Earth Planet. Sci. Lett.*, *493*, 102–117.

Forte, A. M., R. Moucha, N. A. Simmons, S. P. Grand and J. X. Mitrovica (2009), Deep-mantle contributions to the surface dynamics of the North American continent, *Tectonophysics*, *481*(1–4), 3–15, doi:10.1016/j.tecto.2009.06.010.

Fox, M., F. Herman, S. D. Willett, and D. A. May (2014), A linear inversion method to infer exhumation rates in space and time from thermochronometric data, *Earth Surf. Dyn.*, *2*(1), 47–65, doi:10.5194/esurf-2-47-2014.

Fox, M., L. Goren, D. A. May, and S. D. Willett (2014), Inversion of fluvial channels for paleorock uplift rates in Taiwan, *J. Geophys. Res. Earth Surf.*, *119*(9), 1853–1875, doi:10.1002/2014JF003196.

French, S., V. Lekic, and B. Romanowicz (2013), Waveform tomography reveals channeled flow at the base of the oceanic lithosphere, *Science*, *342*(6359), 277–230, doi:10.1038/355437a0.

Gallagher, K. (1995), Evolving temperature histories from apatite fission-track data, *Earth Planet. Sci. Lett.*, *136*(3-4), 421–435, doi:10.1016/0012-821X(95)00197-K.

Gallagher, K. (2012), Transdimensional inverse thermal history modeling for quantitative thermochronology, *J. Geophys. Res. Solid Earth*, *117*(2), doi:10.1029/2011JB008825.

©2018 American Geophysical Union. All rights reserved.

Accepted Article

Gallen, S. F., K. W. Wegmann, and D. W. R. Bohnenstiehl (2013), Miocene rejuvenation of topographic relief in the southern Appalachians, *GSA Today*, *23*(2), 4–10, doi:10.1130/GSATG163A.1.

Gallen, S. F. (2018), Lithologic controls on landscape dynamics and aquatic species evolution in post-orogenic mountains, *Earth Planet. Sci. Lett.*, *493*, 150–160.

Galloway, W., P. Ganey-Curry, X. Li, and R. T. Buffler (2000), Cenozoic depositional history of the Gulf of Mexico basin, *Am. Assoc. Pet. Geol. Bull.*, *84*(11), 1743–1774, doi:10.1306/110801720476.

Galloway, W. E. (2001), Cenozoic evolution of sediment accumulation in deltaic and shore-zone depositional systems, Northern Gulf of Mexico Basin, *Mar. Pet. Geol.*, *18*(10), 1031–1040, doi:10.1016/S0264-8172(01)00045-9.

Galloway, W. E. (2008), Depositional Evolution of the Gulf of Mexico Sedimentary Basin, in *Sediment. Basins World*, vol. 5, edited by A. D. Miall, pp. 505–549, Elsevier, doi:10.1016/S1874-5997(08)00015-4.

Galloway, W. E., T. L. Whiteaker, and P. Ganey-Curry (2011), History of Cenozoic North American drainage basin evolution, sediment yield, and accumulation in the Gulf of Mexico basin, *Geosphere*, *7*(4), 938–973, doi:10.1130/GES00647.1.

Gani, R. M., A. Ranson, D. B.Cross, G. J. Hampson, N. D. Gani and H. Sahoo (2015), Along-strike sequence stratigraphy across the Cretaceous shallow marine to coastal-plain transition, Wasatch Plateau, Utah, U.S.A., *Sediment. Geol.*, *325*, 59–70.

Gans, P. B., and E. L. Miller (1983), Style of mid-Tertiary extension in east-central Nevada, *Geol. excursions overthrust belt Metamorph. core complexes Intermt. Reg. Utah Geol. Miner. Surv. Spec. Stud.*, *59*, 107–139.

Gilbert, G. K. (1877), *Report on the Geology of the Henry Mountains*, U.S. Department of the Interior, Geological Survey of the Rocky Mountains.

Gleadow, A. J. W., and R. W. Brown (1999), Fission track thermochronology and the long-term denudational response to tectonics, *Geomorphol. Glob. Tectonics*, (May), 57–75.

Glotzbach, C. (2015), Deriving rock uplift histories from data-driven inversion of river profiles, *Geology*, *43*, 467–470.

Gohn, G. S. (1988), Late Mesozoic and early Cenozoic geology of the Atlantic Coastal Plain: North Carolina to Florida, in *Atl. Cont. Margin U.S.*, edited by R. E. Sheridan and J. A. Grow, pp. 107–130, Geological Society of America, The Geology of North America, v. I-2, Boulder, CO.

Goren, L., S. D. Willett, F. Herman, and J. Braun (2014), Coupled numerical-analytical approach to landscape evolution modeling, *Earth Surf. Process. Landforms*, *39*(4), 522–545, doi:10.1002/esp.3514.

Gradstein, F. M., J. G. Ogg and F. J. Frits (2012), On the Geological Timescale, *Newsletters Stratigr.*, *2*, 171–188, doi:10.1127/0078-0421/2012/0020

Gray, G. G., R. J. Pottorf, D. A. Yurewicz, K. I. Mahon, D. R. Pevear and R. J. Chuchla (2001), Thermal and chronological record of syn- to post-Laramide burial and exhumation, Sierra Madre Oriental, Mexico, in *AAPG Memoir: The Western Gulf of Mexico Basin: Tectonics, Sedimentary Basins, and Petroleum Systems*, *75* edited by C. Bartolini, R. T. Buffler and A. Cantu-Chapa, pp. 159–181, AAPG.

Green, P. F., I. R. Duddy, A. J. Gleadow, and J. F. Lovering (1989), Apatite Fission-Track Analysis as a Paleotemperature Indicator for Hydrocarbon Exploration, in *Therm. Hist. Sediment. Basins*, edited by N. D. Naeser and T. H. McCulloh, Springer, New York, doi:10.1007/978-1-4612-3492-0_11.

Greenwood, D. R., and S. L. Wing (1995), Eocene continental climates and latitudinal temperature gradients, *Geology*, *23*, 1044–1048

Gregory, K. M., and C. G. Chase (1992), Tectonic significance of paleobotanically estimated climate and altitude of the late Eocene erosion surface, Colorado, *Geology*, *20*, 581–585.

©2018 American Geophysical Union. All rights reserved.

Accepted Article

Gurnis, M. (1993), Phanerozoic marine inundation of continent driven by dynamic topography above subducting slabs, *Nature*, *364*, 590–593.

Gurnis, M., J. X. Mitrovica, J. Ritsema and H. J. van Heijst (2000), Constraining mantle density structure using geological evidence of surface uplift rates: The case of the African Superplume, *Geochem., Geophys. Geosyst.*, *1*(1), doi:10.1029/1999GC000035.

Hager, B. H., and M. A. Richards (1989), Long-wavelength variations in Earth's geoid: Physical models and dynamical implications, *Philos. Trans. R. Soc. A Math. Phys. Eng. Sci.*, *328*(1599), 309–327, doi:10.1098/rsta.1989.0038.

Heaman, L. M., B. A. Kjarsgaard, and R. A. Creaser (2004), The temporal evolution of North American kimberlites, *Lithos*, *76*, 377–397, doi:10.1016/j.lithos.2004.03.047.

Heller, P. L., and L. Liu (2016), Dynamic topography and vertical motion of the U.S. Rocky Mountain region prior to and during the Laramide orogeny, *Geol. Soc. Am. Bull.*, *128*(5-6), 973–988, doi:10.1130/B31431.1.

Heller, P. L., G. Mathers, K. Dueker, and B. Foreman (2013), Far-traveled latest Cretaceous-Paleocene conglomerates of the Southern Rocky Mountains, USA: Record of transient Laramide tectonism, *Bull. Geol. Soc. Am.*, *125*(3-4), 490–498, doi:10.1130/B30699.1.

Henry, C. D., N. H. Hinz, J. E. Faulds, J. P. Colgan, D. A. John, E. R. Brooks, E. J. Cassel, L. J. Garside, D. a. Davis, and S. B. Castor (2012), Eocene-Early Miocene paleotopography of the Sierra Nevada-Great Basin-Nevadaplano based on widespread ash-flow tuffs and paleovalleys, *Geosphere*, doi:10.1130/GES00727.1.

Herman, F., and J. Braun (2006), Fluvial response to horizontal shortening and glaciations: A study in the Southern Alps of New Zealand, *J. Geophys. Res. Earth Surf.*, *111*(1), 1–23, doi:10.1029/2004JF000248.

Herman, F., D. Seward, P. G. Valla, A. Carter, B. Kohn,S. D. Willett, and T. Ehlers (2013), Worldwide acceleration of mountain erosion under a cooling climate, *Nature*, *504*(7480), 423–426, doi:10.1038/nature12877.

Hoggard, M. J., N. White, and D. Al-Attar (2016), Global dynamic topography observations reveal limited influence of large-scale mantle flow, *Nat. Geosci.*, *9*, 456.

Hosman, R. L. (1996), Regional stratigraphy and subsurface geology of Cenozoic deposits, Gulf Coastal Plain, south-central United States, *U.S. Geol. Surv. Prof. Pap. 1416-G*, 1–35.

Howard, A. D. and G. Kerby (1983), Channel changes in badlands, *Geol. Soc. Am. Bull. 94*, 739–752.

Howard, A. D. (1994), A detachment-limited model of drainage basin evolution, *Water Res. Res. 30*, 2261–2285.

Humphreys, E. D. (1995), Post-Laramide removal of the Farallon slab, western United States, *Geology*, *23*(13), 987–990, doi:10.1130/0091-7613(1995)023<0987.

Humphreys, E. D., E. Hessler, K. Dueker, G. L. Farmer, E. Erslev, and T. Atwater (2003), How Laramide-age hydration of North American lithosphere by the Farallon slab controlled subsequent activity in the western United States, *Int. Geol. Rev.*, *45*(7), 575–595, doi:10.2747/0020-6814.45.7.575.

Huntington, K. W., B. P. Wernicke, and J. M. Eiler (2010), Influence of climate change and uplift on Colorado Plateau paleotemperatures from carbonate clumped isotope thermometry, *Tectonics*, *29*(3), 1–19, doi:10.1029/2009TC002449.

Immenhauser, A. (2009), Estimating palaeo-water depth from the physical rock record, *Earth-Science Rev.*, *96*(1-2), 107–139, doi:10.1016/j.earscirev.2009.06.003.

Japsen, P., P. F. Green, J. M. Bonow, A. M. Hinchey, and D. H. C. Wilton, D. (2016), Burial and exhumation history of the Labrador-Newfoundland margin: first observations, *Geol. Surv. Denmark Greenl. Bull.*, *35*, 91-94.

Jeletzky, J. A. (1971), Marine Cretaceous biotic province and paleogeography of western and arctic Canada: illustrated by a detailed study of ammonites, *Geol. Surv. Canada*, *70*, 1–92.

©2018 American Geophysical Union. All rights reserved.

Accepted Article

Johnson, K. R., D. J. Nichols, and J. H. Hartman (2002), Hell Creek Formation: a 2001 synthesis, *in*, The Hell Creek Formation and the Cretaceous-Tertiary boundary in the northern Great Plains: An integrated continental record of the end of the Cretaceous, edited by J. H. Hartman, K. R. Johnson and D. J. Nichols, 503–510, Geological Society of America Special Paper 361, Boulder, CO.

Johnston, S. T. (2001), The Great Alaskan Terrane Wreck: Reconciliation of paleomagnetic and geological data in the Northern Cordillera., *Earth Planet. Sci. Lett.*, *193*, 259–272.

Karlstrom, K. E., R. S. Crow, L. J. Crossey, D. Coblentz, and J. W. Van Wijk (2008), Model for tectonically driven incision of the younger than 6 Ma Grand Canyon, *Geology*, *36*(11), 835–838, doi:10.1130/G25032A.1.

Karlstrom, K. E., D. Coblentz, K. Dueker, W. Ouimet, E. Kirby, J. W. Van Wijk, B. Schmandt, S. A. Kelley, G. Lazear, L. J. Crossey, R. S. Crow, A. Aslan, A. Darling, R. Aster, J. MacCarthy, S. M. Hansen, J. Stachnik, D. F. Stockli, R. V. Garcia, M. Hoffman, R. McKeon, J. Feldman, M. Heizler, and M. S. Donahue (2012), Mantle-driven dynamic uplift of the Rocky Mountains and Colorado Plateau and its surface response: Toward a unified hypothesis, *Lithosphere*, *4*(1), 3–22, doi:10.1130/L150.1.

Karlstrom, K. E., J. P. Lee, S. A. Kelley, R. S. Crow, L. J. Crossey, R. A. Young, G. Lazear, L. S. Beard, J. W. Ricketts, M. Fox, and D. L. Shuster (2014), Formation of the Grand Canyon 5 to 6 million years ago through integration of older palaeocanyons, *Nat. Geosci.*, *7*(3), 239–244, doi:10.1038/ngeo2065.

Karlstrom, K. E., L. J. Crossey, E. Embid, R. Crow, M. Heizler, R. Hereford, L. S. Beard, J. W. Ricketts, S. Cather, and S. Kelley (2017), Cenozoic incision history of the Little Colorado River: Its role in carving Grand Canyon and onset of rapid incision in the past ca. 2 Ma in the Colorado River System, *Geosphere*, *13*(1), 49–81, doi:10.1130/GES01304.1.

Kauffman, E. G., and W. G. E. Caldwell (1993), The Western Interior Basin in space and time, *GAC Spec. Publ.*, *39*(2), 1–30.

Kelley, S. A., and C. E. Chapin (1995), Apatite fission-track thermochronology of the southern Rocky Mountain - Rio Grande rift - western High Plains province, *New Mex. Geol. Soc. F. Conf. Guideb.*, *46*, 87–96.

Ketcham, R. A. (2005), Forward and inverse modeling of low-temperature thermochronometry data, *Rev. Mineral. Geochemistry*, *58*(1), 275–314, doi:10.2138/rmg.2005.58.11.

Kirby, E. and K. Whipple (2001), Quantifying differential rock-uplift rates via stream profile analysis, *Geology*, *29*, 415–418.

Klitgord, K. D., D. R. Hutchinson, and H. Schouten (1988), U.S. Atlantic continental margin; Structural and tectonic framework, in *Atl. Cont. Margin U.S.*, edited by R. E. Sheridan and J. A. Grow, Geological Society of America, The Geology of North America, v. I-2, Boulder, CO.

Klocking, M., N. J. White, J. Maclennan, D. McKenzie and J. G. Fitton (2018), Quantitative relationships between basalt geochemistry, shear wave velocity and asthenospheric temperature beneath western North America, *Geochem., Geophys. Geosys.*, doi:10.1029/2018GC007559.

Koppes, M. N. and D. R. Montgomery (2009), The relative efficacy of fluvial and glacial erosion over modern to orogenic timescales, *Nat. Geosci.*, *2*, 644–647.

Lague, D. (2014), The stream power river incision model: Evidence, theory and beyond, *Earth Surf. Process. Landforms*, *39*(1), 38–61, doi:10.1002/esp.3462.

Lague, D., A. Crave, and P. Davy (2003), Laboratory experiments simulating the geomorphic response to tectonic uplift, *J. Geophys. Res. Solid Earth*, *108*(B1), ETG 3–1–ETG 3–20, doi:10.1029/2002JB001785.

Levander, A., and M. S. Miller (2012), Evolutionary aspects of lithosphere discontinuity structure in the Western U.S., *Geochem., Geophys. Geosys.*, *13*(1), 1–22, doi:10.1029/2012GC004056.

©2018 American Geophysical Union. All rights reserved.

Accepted Article

Levandowski, W., C. H. Jones, L. A. Butcher, and K. H. Mahan (2018), Lithospheric density models reveal evidence for Cenozoic uplift of the Colorado Plateau and Great Plains by lower-crustal hydration, *Geosphere*, *14*(3), 1–15, doi:10.1130/GES01619.1.

Lillegraven, J. A., and L. M. Ostresh (1988), Evolution of Wyoming Early Cenozoic topography and drainage patterns, *Natl. Geogr. Res.*, *4*(3), 303–327.

Lisker, F., B. Ventura and U. A. Glasmacher (2009), Apatite thermochronology in modern geology, *Geol. Soc. London, Spec. Publ.*, *324*, 1–15, 1-23.

Lithgow-Bertelloni, C., and M. Gurnis (1997), Cenozoic subsidence and uplift of continents from time-varying dynamic topography, *Geology*, *25*(8), 735–738, doi:10.1130/0091-7613(1997)025<0735.

Liu, L. (2015), The ups and downs of North America: Evaluating the role of mantle dynamic topography since the Mesozoic, *Rev. Geophys.*, *53*(3), 1022–1049, doi:10.1002/2015RG000489.

Liu, L. (2014), Rejuvenation of Appalachian topography caused by subsidence-induced differential erosion, *Nat. Geosci.*, *7*, 518–523, doi:10.1038/ngeo2187

Liu, L., and M. Gurnis (2010), Dynamic subsidence and uplift of the Colorado Plateau, *Geology*, *38*(7), 663–666, doi:10.1130/G30624.1.

Liu, L., S. Spasojević, and M. Gurnis (2008), Reconstructing Farallon plate subduction beneath North America back to the Late Cretaceous, *Science*, *322*(January), 934–938, doi:10.5061/dryad.5t110.

Liu, S., and D. Nummedal (2004), Late Cretaceous subsidence in Wyoming: Quantifying the dynamic component, *Geology*, *32*(5), 397–400, doi:10.1130/G20318.1.

Lodhia, B. H., G. G. Roberts, A. J. Fraser, S. Fishwick, S. Goes, and J. Jarvis (2018), Continental margin subsidence from shallow mantle convection: Example from West Africa, *Earth Planet. Sci. Lett.*, *481*, 350–361, doi:10.1016/j.epsl.2017.10.024.

Loget, N., and J. Van Den Driessche (2009), Wave train model for knickpoint migration, *Geomorphology*, *106*(3-4), 376–382, doi:10.1016/j.geomorph.2008.10.017.

Luke, J. C. (1972), Mathematical models for landform evolution, *Journal of Geophysical Research*, *77*(14), 2460–2464.

Mackey, B. H., J. S. Scheingross, M. P. Lamb, and K. A. Farley (2014), Knickpoint formation, rapid propagation, and landscape response following coastal cliff retreat at the last interglacial sea-level highstand: Kaua'i, Hawai'i, *Bull. Geol. Soc. Am.*, *126*(7-8), 925–942, doi:10.1130/B30930.1.

Matmon, A., P. R. Bierman, J. Larsen, S. Southworth, M. Pavich, and M. Caffee (2003), Temporally and spatially uniform rates of erosion in the southern Appalachian Great Smoky Mountains, *Geology*, *31*(2), 155–158, doi:10.1130/0091-7613(2003)031<0155:TASURO>2.0.CO;2.

Marquez, A., R. Oyarzun, M. Doblas, and S. P. Verma (1999), Alkalic (ocean-island basalt type) and calc-alkalic volcanism in the Mexican volcanic belt: A case for plume-related magmatism and propagating rifting at an active margin?, *Geology*, *27*(1), 51–54.

McKenna, M. C., and J. D. Love (1972), High-level strata containing Early Miocene mammals on the Bighorn Mountains, Wyoming, *Am. Museum Novit.*, *2490*, 31.

McKenzie, D. (2003), Estimating T_e in the presence of internal loads, *J. Geophys. Res. Solid Earth*, *108*(B9), 1–21, doi:10.1029/2002JB001766.

McKenzie, D., J. Jackson, and K. Priestley (2005), Thermal structure of oceanic and continental lithosphere, *Earth Planet. Sci. Lett.*, *233*(3-4), 337–349, doi:10.1016/j.epsl.2005.02.005.

McKeon, R. E., P. K. Zeitler, F. J. Pazzaglia, B. D. Idleman, and E. Enkelmann (2014), Decay of an old orogen: Inferences about Appalachian landscape evolution from low-temperature thermochronology, *Bull. Geol. Soc. Am.*, *126*(1-2), 31–46, doi:10.1130/B30808.1.

McMillan, M. E., C. L. Angevine, and P. L. Heller (2002), Postdepositional tilt of the Miocene-Pleistocene Ogallala Group on the western Great Plains: Evidence of Late Cenozoic uplift of the Rocky Mountains, *Geol. Soc. Am.*, *30*, 63–66.

©2018 American Geophysical Union. All rights reserved.

Accepted Article

McMillan, M. E., P. L. Heller, and S. L. Wing (2006), History and causes of post-Laramide relief in the Rocky Mountain orogenic plateau, *Bull. Geol. Soc. Am.*, *118*(3-4), 393–405, doi:10.1130/B25712.1.

McQuarrie, N., and C. G. Chase (2000), Raising the Colorado Plateau; discussion and reply, *Geology*, *28*(8), 767–768, doi:10.1130/0091-7613(2000)028<0091:RTCP>2.0.CO;2.

Menke, W., P. Skryzalin, V. Levin, T. Harper, F. Darbyshire, and T. Dong (2016), The Northern Appalachian Anomaly: A modern asthenospheric upwelling, *Geophys. Res. Lett.*, *43*, 10173–10179, doi:10.1002/ 2016GL070918.

Merewether, E. A., and K. C. McKinney (2015), Composite biostratigraphic outcrop sections for Cretaceous Formations along a south-trending transect from northwestern Montana to northwestern New Mexico, *USGS*, *1258*, 20151,087.

Miller, K. G. (2005), The Phanerozoic record of global sea-level change, *Science*, *310*(5752), 1293–1298, doi:10.1126/science.1116412.

Miller, S. R., P. B. Sak, E. Kirby, and P. R. Bierman (2013), Neogene rejuvenation of central Appalachian topography: Evidence for differential rock uplift from stream profiles and erosion rates, *Earth Planet. Sci. Lett.*, *369-370*, 1–12, doi:10.1016/j.epsl.2013.04.007.

Milliken, K. T., M. D. Blum, J. W. Snedden, and W. E. Galloway (2018), Application of fluvial scaling relationships to reconstruct drainage basin evolution and sediment routing for the Cretaceous and Paleocene of the Gulf of Mexico, *Geosphere*, *14*(2), 749–767, doi:10.1130/GES01374.1.

Milliman, J., and K. Farnsworth (2011), River Discharge to the Coastal Ocean: A Global Synthesis, *Cambridge Univ. Press. Cambridge, U.K*, p. 392, doi:10.5670/oceanog.2011.108.

Missimer, T. M., and R. G. Maliva (2017), Late Miocene fluvial sediment transport from the southern Appalachian Mountains to southern Florida: An example of an old mountain belt sediment production surge, *Sedimentology*, *64*(7), 1846–1870, doi:10.1111/sed.12377.

Mitrovica, J. X., C. Beaumont, and G. T. Jarvis (1989), Tilting of continental interiors by the dynamical effects of subduction, *Tectonics*, *8*(5), 1079–1094, doi:10.1029/TC008i005p01079.

Mix, H. T., A. Mulch, M. L. Kent-Corson, and C. P. Chamberlain (2011), Cenozoic migration of topography in the North American Cordillera, *Geology*, *39*(1), 87–90, doi:10.1130/G31450.1.

Molnar, P., and P. England (1990), Late Cenozoic uplift of mountain ranges and global climate change: chicken or egg?, *Nature*, *346*(6279), 29–34, doi:10.1038/346029a0.

Molnar, P., P. C. England, and C. H. Jones (2015), Mantle dynamics, isostasy, and the support of high terrain, *J. Geophys. Res.*, *120*, 1932–1957, doi:10.1002/2014JB011724.

Montgomery, D. R., and J. López-Blanco (2003), Post-Oligocene river incision, southern Sierra Madre Occidental, Mexico, *Geomorphology*, *55*(1-4), 235–247, doi:10.1016/S0169-555X(03)00142-9.

Morrison, R. B. (1991), Quaternary stratigraphic, hydrologic, and climatic history of the Great Basin, with emphasis on Lakes Lahontan, Bonneville, and Tecopa, *Quaternary Nonglacial Geology: Conterminous US*, *2*, 283–320, doi:10.1002/2014JB011724.

Moucha, R., A. M. Forte, J. X. Mitrovica, D. B. Rowley, S. Quéré, N. A. Simmons, and S. P. Grand (2016), Dynamic topography and long-term sea-level variations: There is no such thing as a stable continental platform, *Earth Planet. Sci. Let.*, *271*(1–4), 101–108.

Naeser, C. W., N. D. Naeser, W. L. Newell, S. Southworth, L. E. Edwards, and R. E. Weems (2016), Erosional and depositional history of the Atlantic passive margin as recorded in detrital zircon fission-track ages and lithic detritus in Atlantic Coastal Plain sediments, *Am. J. Sci.*, *316*(2), 110–168, doi:10.2475/02.2016.02.

Naeser, N. D., C. W. Naeser, C. S. Southworth, B. A. Morgan, and A. P. Schultz (2004), Paleozoic to Recent tectonic and denudation history of rocks in the Blue Ridge

©2018 American Geophysical Union. All rights reserved.

Accepted Article

Province, central and southern Appalachians – Evidence from fission-track thermochronology, *Geol. Soc. Am. Abstr. with Programs*, *36*(2).

Nassichuk, W. W., and D. J. McIntyre (1995), Cretaceous and Tertiary fossils discovered in kimberlites at Lac de Gras in the Slave Province, Northwest Territories, *Curr. Res. - Geol. Surv. Canada*, *B*, 109–114.

Nereson, A., J. Stroud, K. Karlstrom, M. Heizler, and W. McIntosh (2013), Dynamic topography of the western Great Plains: Geomorphic and $^{40}Ar/^{39}Ar$ evidence for mantle-driven uplift associated with the Jemez lineament of NE New Mexico and SE Colorado, *Geosphere*, *9*(3), 521–545, doi:10.1130/GES00837.1.

Nurkowski, J. R. (1984), Coal quality, coal rank variation and its relation to reconstructed overburden, Upper Cretaceous and Tertiary plains coals, Alberta, Canada, *Am. Assoc. Pet. Geol. Bull.*, *68*(3), 285–295.

Obradovich, J. D., and W. A. Cobban (1975), A time-scale for the Late Cretaceous of the Western Interior of North America, *Geol. Assoc. Canada Spec. Pap.*, *13*, 31–54.

Olsson, R. K., T. G. Gibson, H. J. Hansen, and J. P. Owens (1988), Geology of the northern Atlantic coastal plain: Long Island to Virginia, in *Atl. Cont. Margin U.S.*, edited by R. E. Sheridan and J. A. Grow, pp. 87–105, Geological Society of America, The Geology of North America, v. I-2, Boulder, CO.

O'Sullivan, P. B., and Currie, L. D., 1996. Thermotectonic history of Mt Logan, Yukon Territory, Canada: Implications of multiple episodes of middle to late Cenozoic denudation, *Earth and Planetary Science Letters*, *144*, 251–261.

O'Sullivan, P. B., and L. S. Lane (1997), Early Tertiary thermotectonic history of the northern Yukon and adjacent Northwest Territories, Arctic Canada, *Can. J. Earth Sci.*, *34*(10), 1366–1378, doi:10.1139/e17-109.

Pang, M., and D. Nummedal (1995), Flexural subsidence and basement tectonics of the Cretaceous Western Interior basin, United States, *Geology*, *23*(2), 173–176.

Parker, R. L. (1994), Geophysical Inverse Theory, *Princeton University Press*.

Paul, J. D., G. G. Roberts, and N. White (2014), The African landscape through space and time, *Tectonics*, *33*(6), 898–935, doi:10.1002/2013TC003479.

Pavich, M. J., L. Brown, J. N. Valette-Silver, J. Klein, and R. Middleton (1985), ^{10}Be analysis of a Quaternary weathering profile in the Virginia Piedmont, *Geology*, *13*(1), 39–41.

Pazzaglia, F. J., and M. T. Brandon (1996), Macrogeomorphic evolution of the post-Triassic Appalachian mountains determined by deconvolution of the offshore basin sedimentary record, *Basin Res.*, *8*(1996), 1–24.

Pazzaglia, F. J., and W. Gardner (1994), Late Cenozoic flexural deformation of the middle U.S. Atlantic passive margin, *J. Geodyn.*, *99*(B6), 12,143–12,157.

Peel, F. J., C. J. Travis, and J. R. Hossback (1995), Genetic structural provinces and salt tectonics of the Cenozoic offshore U.S. Gulf of Mexico: a preliminary analysis, in *Salt tectonics a Global. Perspective*, edited by M. P. A. Jackson, D. G. Roberts, and S. Snelson, pp. 153–175, AAPG Memoir.

Peyton, S. L., and B. Carrapa (2013), An overview of low-temperature thermochronology in the Rocky Mountains and its application to petroleum system analysis, *AAPG Stud. Geol.*, *65*, 37–70, doi:10.1306/13381689St653578.

Poag, C. W., and W. D. Sevon (1989), A record of Appalachian denudation in postrift Mesozoic and Cenozoic sedimentary deposits of the U.S. Middle Atlantic continental margin, *Geomorphology*, *2*(1-3), 119–157, doi:10.1016/0169-555X(89)90009-3.

Portenga, E. W., P. R. Bierman, D. M. Rizzo, and D. H. Rood (2013), Low rates of bedrock outcrop erosion in the Central Appalachian mountains inferred from in situ 10Be, *Bull. Geol. Soc. Am.*, *125*(1-2), 201–215, doi:10.1130/B30559.1.

Priestley, K., and D. McKenzie (2006), The thermal structure of the lithosphere from shear wave velocities, *Earth Planet. Sci. Lett.*, *244*(1-2), 285–301, doi:10.1016/j.epsl.2006.01.008.

©2018 American Geophysical Union. All rights reserved.

Accepted Article

Prince, P. S., and J. A. Spotila (2013), Evidence of transient topographic disequilibrium in a landward passive margin river system: Knickpoints and paleo-landscapes of the New River basin, southern Appalachians, *Earth Surf. Process. Landforms*, *38*(14), 1685–1699, doi:10.1002/esp.3406.

Pritchard, D., G. G. Roberts, N. J. White, and C. N. Richardson (2009), Uplift histories from river profiles, *Geophys. Res. Lett.*, *36*(24), 1–5, doi:10.1029/2009GL040928.

Ramirez-Herrera, M. T., V. Kostoglodov, and J. Urrutia-Fucugauchi (2011), Overview of recent coastal tectonic deformation in the Mexican subduction zone, *Pure Appl. Geophys.*, *168*(8-9), 1415–1433, doi:10.1007/s0024-010-0205-y.

Reed Jr., J. C., J. O.Wheeler and B. E. Tucholke (2005), Geologic Map of North America, *Geol. Soc. Am., Decade of North American Geology*.

Reiners, P. W., and M. T. Brandon (2006), Using thermochronology to understand orogenic erosion, *Annu. Rev. Earth Planet. Sci.*, *34*, 419–466, doi:10.1146/annurev.earth.34.031405.125202.

Rengers, F. K., and G. E. Tucker (2014), Analysis and modeling of gully headcut dynamics, North American high plains, *J. Geophys. Res. Earth Surf.*, *119*(5), 983–1003, doi:10.1002/2013JF002962.

Repasch, M., K. Karlstrom, M. Heizler, and M. Pecha (2017), Birth and evolution of the Rio Grande fluvial system in the past 8 Ma: Progressive downward integration and the influence of tectonics, volcanism, and climate, *Earth-Science Rev.*, *168*, 113–164, doi:10.1016/j.earscirev.2017.03.003.

Ritsema, J., A. Deuss, H. J. van Heijst, and J. H. Woodhouse (2011), S40RTS: a degree-40 shear-velocity model for the mantle from new Rayleigh wave dispersion, teleseismic traveltime and normal-mode splitting function measurements, *Geophys. J. Int.*, *184*(3), 1223–1236.

Roberts, G. G., and N. White (2010), Estimating uplift rate histories from river profiles using African examples, *J. Geophys. Res. Solid Earth*, *115*(2), 1–24, doi:10.1029/2009JB006692.

Roberts, G. G., N. J. White, G. L. Martin-Brandis, and A. G. Crosby (2012a), An uplift history of the Colorado Plateau and its surroundings from inverse modeling of longitudinal river profiles, *Tectonics*, *31*(4), 1–25, doi:10.1029/2012TC003107.

Roberts, G. G., J. D. Paul, N. White, and J. Winterbourne (2012b), Temporal and spatial evolution of dynamic support from river profiles: A framework for Madagascar, *Geochemistry, Geophys. Geosystems*, *13*(4), 1–23, doi:10.1029/2012GC004040.

Roberts, G. G., N. White, M. J. Hoggard, P. W. Ball, and C. Meenan (2018), A Neogene history of mantle convective support beneath Borneo, *Earth Planet. Sci. Lett.*, *496*, 142–158, doi:10.1016/j.epsl.2018.05.043.

Roberts, G. G. (2019), Scales of similarity and disparity between drainage networks, *Geophys. Res. Lett.*, doi: 10.1029/2019GL082446.

Roberts, G. G., N. J. White, and B. H. Lodhia (2019), Generation and scaling of longitudinal river profiles. *Journal of Geophysical Research*, doi:10.1029/2018JF004796.

Roberts, L. N., and M. A. Kirschbaum (1995), Paleogeography of the Late Cretaceous of the Western Interior of middle North America – Coal distribution and sediment accumulation, *U.S. Geol. Surv. Prof. Pap. 1561*, p. 115.

Roden-Tice, M. K., J. D. Eusden, and R. P. Wintsch (2012), Apatite fission-track evidence for the Cretaceous development of kilometer-scale relief and steady-state Tertiary topography in New England, *Geomorphology*, *141-142*, 114-120, doi:10.1016/j.geomorph.2011.12.029.

Rosenbloom, N. A. and R. S. Anderson, Hillslope and channel evolution in a marine terraced landscape, Santa Cruz, California, *J. Geophys. Res.*, *99*, 13–14.

Rowley, D. B., A. M. Forte, R. Moucha, J. X. Mitrovica, N. A. Simmons, and S. P. Grand (2013), Dynamic topography change of the eastern United States since 3 million years ago., *Science*, *340*(6140), 1560–3, doi:10.1126/science.1229180.

©2018 American Geophysical Union. All rights reserved.

Accepted Article

Roy, M., T. H. Jordan, and J. L. Pederson (2009), Colorado Plateau magmatism and uplift by warming of heterogeneous lithosphere., *Nature*, *459*(7249), 978–82, doi:10.1038/nature08052.

Royden, L., and J. T. Perron (2013), Solutions of the stream power equation and application to the evolution of river longitudinal profiles, *J. Geophys. Res. Earth Surf.*, *118*(2), 497–518, doi:10.1002/jgrf.20031.

Rudge, J. F., G. G. Roberts, N. J. White, and C. N. Richardson (2015), Uplift histories of Africa and Australia from linear inverse modeling of drainage inventories, *J. Geophys. Res. F Earth Surf.*, *120*(5), 894–914, doi:10.1002/2014JF003297.

Sahagian, D. (1987), Epeirogeny and eustatic sea level changes as inferred from Cretaceous shoreline deposits: Applications to the central and western United States, *J. Geophys. Res. Solid Earth*, *92*, 4895–4904, doi:10.1029/JB092iB06p04895.

Salles, T. (2015), Badlands: A parallel basin and landscape dynamics model, *SoftwareX*, *5*, 195–202, doi:10.1016/j.softx.2016.08.005.

Salles, T., N. Flament, and D. Muller (2017), Influence of mantle flow on the drainage of eastern Australia since the Jurassic Period, *Geochem. Geophys. Geosys.*, *18*, 280–305, doi:10.1002/2016GC006617.

Schaeffer, A. J. and Lebedev, S. (2013), Global shear speed structure of the upper mantle and transition zone, *Geophys. J. Int.*, *149*, 417–449.

Schildgen, T. F., P. A. van der Beek, H. D. Sinclair, and R. C. Thiede (2018), Spatial correlation bias in late-Cenozoic erosion histories derived from thermochronology, *Nature*, *559*(7712), 89–93, doi:10.1038/s41586-018-0260-6.

Self, R. P. (1977), Longshore variation in beach sands, Nautla Area, Veracruz, Mexico, *J. Sediment. Res.*, *47*(4), 1437–1443, doi:10.1306/212F7388-2B24-11D7-8648000102C1865D.

Setterholm, D. R. (1994), The Cretacous rocks of southwestern Minnesota: Reconstructions of a marine to nonmarine transition along the eastern margin of the Western Interior Seaway, in *Perspect. East. Margin Cretacous West. Inter. Seaw.*, edited by G. W. Shurr, G. W. Ludvigson, and R. H. Hammond, pp. 97–110, Geological Society of America Special Paper 287, Boulder, CO.

Shen, W., and M. H. Ritzwoller (2016), Crustal and uppermost mantle structure beneath the United States, *J. Geophys. Res. Solid Earth Solid Earth*, *121*, 4306–4342, doi:10.1002/2016JB012887.

Sklar, L., and W. E. Dietrich (1998), River longitudinal profiles and bedrock incision models: Stream power influence of sediment supply, *Rivers Over Rock Fluv. Process. Bedrock Channels Geophys. Monogr.*, *107*, 237–260.

Sklar, L. S., and W. E. Dietrich (2001), Sediment and rock strength controls on river incision into bedrock, *Geology*, *29*(12), 1087–1090.

Revised by Slone, J., C. D. Henry, M. Hopkins and S. Ludington. Original database by Zartman, R. E., C. A. Bush and C. Abston (2003), National Geochronological Database, *U. S. Geological Survey Open-file Report*, *03-236*, https://pubs.usgs.gov/of/2003/0236.

Smith, A. G., D. G. Smith, and B. M. Funnell (1994), *Atlas of Mesozic and Cenozoic Coastlines*, 99 pp., Cambridge University Press.

Snyder, W. S., W. R. Dickinson, and M. L. Silberman (1976), Tectonic implications of space-time patterns of Cenozoic magmatism in the Western United States, *Earth Planet. Sci. Lett.*, *32*, 91–106.

Snyder, N. P., K. Whipple, G. Tucker, and D. Merritts (2000), Landscape response to tectonic forcing: DEM analysis of stream profiles in the Mendocino triple junction region, northern California, *Geol. Soc. Am. Bull.*, *112*(8), 1250–1263, doi:10.1130/0016-7606(2000)112<1250:LRTTFD>2.3.CO;2.

Spasojević, S., and M. Gurnis (2012), Sea level and vertical motion of continents from dynamic earth models since the Late Cretaceous, *Am. Assoc. Pet. Geol. Bull.*, *96*(11), 2037–2064, doi:10.1306/03261211121.

©2018 American Geophysical Union. All rights reserved.

Accepted Article

Spasojević, S., L. Liu and M. Gurnis (2009), Adjoint models of mantle convection with seismic, plate motion, and stratigraphic constraints: North America since the Late Cretaceous, *Geochem., Geophys. Geosys.*, *10*, Q05W02, doi:10.1029/2008GC002345.

Spencer, J. E. (1996), Uplift of the Colorado Plateau due to lithosphere attenuation during Laramide low-angle subduction, *J. Geophys. Res.*, *101*, 13,595, doi:10.1029/96JB00818.

Stephenson, S. N., G. G. Roberts, M. J. Hoggard, and A. C. Whittaker (2014), A Cenozoic uplift history of Mexico and its surroundings from longitudinal river profiles, *Geochem. Geophys. Geosys.*, *15*, 4734–4758, doi:10.1002/2014GC005425.

Stone, D. S. (1993), Basement-involved thrust-generated folds as seismically imaged in the subsurface of the central Rocky Mountain foreland, *Geol. Soc. Am. Spec. Pap.*

Tachikawa, T., M. Kaku, A. Iwasaki, D. Gesch, M. Oimoen, Z. Zhang, J. Danielson, T. Krieger, B. Curtis, J, Haase, M. Abrams, R. Crippen and C. Carabajal (2011), *ASTER Digital Elevation Model Version 2 - Summary of validation results*.

Tapley, B., J. Ries, S. Bettadpur, D. Chambers, M. Cheng, F. Condi, B. Gunter, Z. Kang, P. Nagel, R. Pastor, T. Pekker, S. Poole and F. Wang (2005), GGM02 - An improved Earth gravity field model from GRACE, *J. Geod.*, *79*, 467–478, doi:10.1007/s00190-005-0480-z

Taylor, J. P., and P. G. Fitzgerald (2011), Low-temperature thermal history and landscape development of the eastern Adirondack Mountains, New York: Constraints from apatite fission-track thermochronology and apatite (U-Th)/He dating, *Bull. Geol. Soc. Am.*, *123*(3-4), 412–426, doi:10.1130/B30138.1.

Thompson, G. A., and M. L. Zoback (1979), Regional geophysics of the Colorado Plateau, *Tectonophysics*, *61*(1-3), 149–181, doi:10.1016/0040-1951(79)90296-8.

van Wijk, J. W., W. S. Baldridge, J. van Hunen, S. Goes, R. Aster, D. D. Coblentz, S. P. Grand, and J. Ni (2010), Small-scale convection at the edge of the Colorado Plateau: Implications for topography, magmatism, and evolution of Proterozoic lithosphere, *Geology*, *38*, 611–614.

Wakabayashi, J., and T. L. Sawyer (2001), Stream Incision , Tectonics , Uplift , and Evolution of Topography of the Sierra Nevada , California, *J. Geol.*, *109*(5), 539–562.

Weissel, J. K. and M. A. Seidl (1998), Inland propagation of erosional escarpments and river profile evolution across the southeast Australian passive continental margin, *Geophysical Monograph - American Geophysical Union*, *107*, 189–206.

Wernicke, B. P. (1992), Cenozoic extensional tectonics of the U.S. Cordillera, in *Cordilleran Orogen Conterminous U.S.*, edited by B. C. Burchfeil, P. W. Lipman, and M. L. Zoback, pp. 553–581, Geological Society of America, The Geology of North America, v. G-3, Boulder, CO.

Whipple, K. X., and G. E. Tucker (1999), Dynamics of the stream-power river incision model: Implications for height limits of mountain ranges, landscape response timescales, and research needs, *J. Geophys. Res. Solid Earth*, *104*(B8), 17,661–17,674, doi:10.1029/1999JB900120.

Whittaker, A. C., P. A. Cowie, M. Attal, G. E. Tucker and G. Roberts (2007), Bedrock channel adjustment to tectonic forcing: Implications for predicting river incision rates, *Geology*, *35*, 103–106, doi:10.1130/G23106A.1.

Whittaker, A. C., and S. J. Boulton (2012), Tectonic and climatic controls on knickpoint retreat rates and landscape response times, *J. Geophys. Res. Earth Surf.*, *117*, 1–19.

Wickert, A. D. (2016), Reconstruction of North American drainage basins and river discharge since the Last Glacial Maximum, *Earth Surf. Dyn.*, *4*(4), 831–869, doi:10.5194/esurf-4-831-2016.

Willett, S. D., S. W. McCoy, J. T. Perron, L. Goren, and C.-Y. Chen (2014), Dynamic Reorganization of River Basins, *Science*, *343*(6175), 1248,765–1248,765, doi:10.1126/science.1248765.

Willett, S. D., S. W. McCoy, and H. W. Beeson (2018), Transience of the North American High Plains landscape and its impact on surface water, *Nature*, doi:10.1038/s41586-018-0532-1.

©2018 American Geophysical Union. All rights reserved.

Accepted Article

Wilson, D., R. Aster, J. Ni, S. Grand, M. West, W. Gao, W. S. Baldridge, and S. Semken (2005), Imaging the seismic structure of the crust and upper mantle beneath the Great Plains, Rio Grande Rift, and Colorado Plateau using receiver functions, *J. Geophys. Res. Solid Earth*, *110*(5), 1–14, doi:10.1029/2004JB003492.

Winn, C., K. E. Karlstrom, D. L. Shuster, S. Kelley, and M. Fox (2017), 6 Ma age of carving Westernmost Grand Canyon: Reconciling geologic data with combined AFT, (U–Th)/He and $^{4}He/^{3}He$ thermochronologic data, *Earth Planet. Sci. Lett.*, *474*, doi:10.1016/j.epsl.2017.06.051.

Wobus, C. W., K. X. Whipple, E. Kirby, N. Snyder, J. Johnson, K. Spyropolou, B. Crosby, and D. Sheehan (2006), Tectonics from topography: procedures, promise, pitfalls, in *Tectonics, Climate, and Landscape Evolution: Geological Society of America Special Paper 398*, edited by Willett, S. D., N. Hovius, M. T. Brandon and D. M. Fisher, *Penrose Conference Series*, 55–74, doi:10.1130/2006.2398(04).

Wolfe, J. A., C. E. Forest, and P. Molnar (1998), Paleobotanical evidence of Eocene and Oligocene paleoaltitudes in midlatitude western North America, *Bull. Geol. Soc. Am.*, *110*(5), 664–678, doi:10.1130/0016-7606(1998)110<0664:PEOEAO>2.3.CO;2.

Ziegler, A., D. Rowley, A. Lottes, D. Sahagian, M. Hulver, and T. Gierlowski (1985), Paleogeographic interpretation: with an example from the mid-Cretaceous, *Annu. Rev. Earth Planet. Sci.*, *13*, 385–425, doi:10.1146/annurev.earth.13.1.385.

Zoback, M. L., G. A. Thompson, and R. E. Anderson (1981), Cainozoic evolution of the state of stress and style of tectonism of the Basin and Range province of the western United States, *Philos. Trans. R. Soc. London. Ser. A, Math. Phys. Sci.*, *300*(1454), 407–434.

©2018 American Geophysical Union. All rights reserved.